UAV-enabled Multi-pair Massive MIMO-NOMA Relay Systems with Low-Resolution ADCs/DACs

Xingwang Li, *Senior Member, IEEE,* Mingyu Zhang, Hui Chen, Congzheng Han, *Senior Member, IEEE,* Lihua Li, *Member, IEEE,* Dinh-Thuan Do, *Senior Member, IEEE,* Shahid Mumtaz, *Senior Member, IEEE,* and Arumugam Nallanathan, *Fellow, IEEE*

***Abstract*—In this paper, we consider an unmanned aerial vehicle (UAV)-enabled massive multiple-input multiple-out (MIMO) non-orthogonal multiple access (NOMA) full-duplex (FD) two-way relay (TWR) system with low-resolution analog-to-digital converters/digital-to-analog converters (ADCs/DACs), where the UAV provides services for multi-pair ground users (GUs). By employing maximum ratio combining/maximum ratio transmission (MRC/MRT), the approximate closed-form expressions for sum spectrum/energy efficiency (SE/EE) with imperfect channel state information (CSI), imperfect successive interference cancellation (SIC) and quantization noise are derived. To evaluate the effects of the parameters on system performance, the asymptotic analysis and the power scaling laws are further provided. The numerical results verify the accuracy of theoretical analysis and show that the interference and noise can be effectively eliminated by deploying large-scale antennas, adopting larger Rician factors, and applying proper power scaling law. We also demonstrate that the proposed system can obtain better SE by adjusting the height of the UAV. Moreover, the system performance is related to the ADCs/DACs quantization bits, where the SE saturation values increase with the increasing number of quantization bits, while the EE first increases and then decreases. Finally, the SE/EE trade-off at low precision ADCs/DACs can be achieved by choosing the appropriate number of quantization bits, and the trade-off region grows as Rician factor increases.**

***Index Terms*—Unmanned aerial vehicle (UAV), massive multiple-input multiple-out (MIMO), non-orthogonal multiple access (NOMA), two-way relay (TWR), low-resolution ADCs/DACs.**

I. Introduction

UNMANNED aerial vehicles (UAVs) have attracted widespread attention for the high mobility, ease of deployment, and low cost, which can provide solutions for application scenarios with terrestrial communication loads, such as by deploying UAVs to meet network reconstruction requirements after major natural disasters and the sudden increasing communication needs for major holiday gatherings [1]. UAV-assisted communication is recognized as a potential indispensable technology in the beyond-fifth generation/sixth generation (B5G/6G) communication networks [2]–[4]. Compared with conventional terrestrial communications, the UAV-ground channel has an inherent advantage of stronger line-of-sight (LoS) links, which is more attractive to provide high transmission rates and reliable wireless connectivity [5]. On the other hand, massive multiple-input multiple-output (MIMO), non-orthogonal multiple access (NOMA) and full-duplex (FD) are also promising technologies for future mobile networks. Through massive MIMO, the system spectrum efficiency (SE) and energy efficiency (EE) can be significantly enhanced [6], [7]. By invoking superposition coding (SC) and successive interference cancellation (SIC), NOMA can achieve higher spectrum utilization and larger system capacity than conventional orthogonal multiple access (OMA) [8], [9]. The FD mode can theoretically achieve double the transmission rate than half-duplex (HD) one [10].

The integration of massive MIMO, NOMA and FD into UAV communication networks can effectively relieve the capacity pressure caused by ultra-dense access and improve the quality-of-service of wireless communication. Besides, two-way transmission can further improve the SE of UAV relay systems [11]. Some related studies combining these technologies have been carried out in [12]–[14]. All the aforementioned works consider the use of a dedicated radio frequency (RF) chain on each antenna of the UAV. However, in practical implementation of UAV-enabled FD massive MIMO systems, deploying large-scale antennas will significantly complicate the hardware design, since the related hardware cost and power consumption are unaffordable. Specifically, each antenna element requires an analog-to-digital converter/digital-to-analog converter (ADC/DAC) unit [15]. This suggests that the increase of antennas number leads to the increase in ADC/DAC converters. The power consumption of the analog-digital converters is linearly related to the sampling frequency and exponentially related to the resolution [16]. To address this problem, an effective way is to employ low-resolution ADCs/DACs, which has the benefits of cost effectiveness, energy saving and engineering simplicity.

Recently, there are a lot of works on applying low-resolution ADCs/DACs to FD massive MIMO systems [17]–[22]. In [17], the authors analyzed the impacts of low-resolution ADCs and loop interference on the achievable SE of a multi-user FD

Xingwang Li, Mingyu Zhang and Hui Chen are with the School of Physics and Electronic Information Engineering, Henan Polytechnic University, Jiaozuo, China (email:lixingwangbupt@gmail.com, zhangmingyu89@163.com, hchen@hpu.edu.cn).

Congzheng Han is Middle Atmosphere and Global environment Observation (LAGEO) Institute of Atmospheric Physics, Chinese Academy of Sciences, Beijing, 100029, China (e-mail: c.han@mail.iap.ac.cn).

Lihua Li is with the State Key Laboratory of Networking and Switching Technology, Beijing University of Posts and Telecommunications, Beijing 100088, China (e-mail: lilihua@bupt.edu.cn).

Dinh-Thuan Do is with the School of Engineering, University of Mount Union, Alliance OH 44601, USA (email:doth@mountunion.edu).

Shahid Mumtaz is with Instituto de Telecomunicacoes, Aveiro, Portugal (email:smumtaz@av.it.pt).

Arumugam Nallanathan is with School of Electronic Engineering and Computer Science, Queen Mary University of London, London, U.K. (email: a.nallanathan@qmul.ac.uk).

massive MIMO amplify-and-forward (AF) relaying systems, which utilized the maximum ratio combining/maximum ratio transmission (MRC/MRT) and zero-forcing reception/zero-forcing transmission. Considering channel estimation, the authors in [18] derived the exact and approximate closed-form expressions for the achievable sum rate (ASR) of the systems similar to [17] and provided the optimal relay power allocation scheme. The rate performance of a FD massive MIMO relaying system over Rician fading channels with low-resolution ADCs was studied in [19]. Extending to heterogeneous network, the authors in [20] considered the network backhaul implementation of low-resolution ADCs FD massive MIMO systems, and investigated the SE/EE under imperfect channel state information (CSI) over Rician fading channels. The authors in [21] and [22] investigated the uplink/downlink (UL/DL) rates of the FD massive MIMO systems with low-resolution ADCs/DACs under perfect CSI and imperfect CSI over Rician fading channels, and the EE was also discussed. All these studies are based on unidirectional OMA. Moreover, channel estimation was performed in [18], [20]–[22], and only [18] considered the effect of quantization error on channel estimation, but it merely studied the effect of low-resolution ADCs.

Motivated by the above discussion and relying on the research gap that still exist in the literature, which is summarized in Table I. To bridge this gap, this paper analyzes the effect of quantization error on the UL and DL channel estimation, and studies the SE and EE performance of UAV-enabled multi-pair massive MIMO-NOMA relay systems, where the two-way shared FD UAV is configured with massive antennas in the presence of low-resolution ADCs/DACs. The main contributions are listed as follows:

- We consider a low-resolution ACD/DAC architecture for UAV-enabled FD massive MIMO-NOMA two-way relay (TWR) systems. The UAV employs low-resolution ADCs and low-resolution DACs on the receive and transmit antennas, respectively. This double quantized system model complements the vacancy in existing research on UAV-aided MIMO communications, which can significantly improve SE performance with small power consumption and low hardware cost.
- We investigate the SE and EE performance under imperfect CSI, imperfect SIC and low-resolution ADCs/DACs. More precisely, by employing MRC/MRT, the closed-form approximate expressions of the sum SE and total EE are derived. The effects of the transmit power of GUs/UAV, the number of UAV antennas, the height of the UAV, the number of quantization bits and the Rician factor on the system performance are further analyzed.
- Based on approximation expressions, we present some asymptotic analysis, and characterize the power scaling law. The results show that by appropriately adjusting the UAV altitude, increasing the value of Rician factor and the number of UAV antennas can effectively compensate the SE loss caused by quantization noise. We also find that despite the use of low-resolution ADCs/DACs, employing massive antennas at the UAV can provide significant power savings.
- In the simulation section, we confirm that with low-resolution ADC/DAC architecture, the proposed massive MIMO-NOMA FD TWR system has an appreciable SE gain compared to the corresponding OMA and/or HD system. Moreover, we provide the SE/EE trade-off for different quantization bits. The optimal number of quantization bits and the required UAV antennas to maximize EE are illustrated. We further demonstrate that the proposed system works better in Rician fading channels with stronger LoS component in the presence of low-resolution ADCs/DACs.

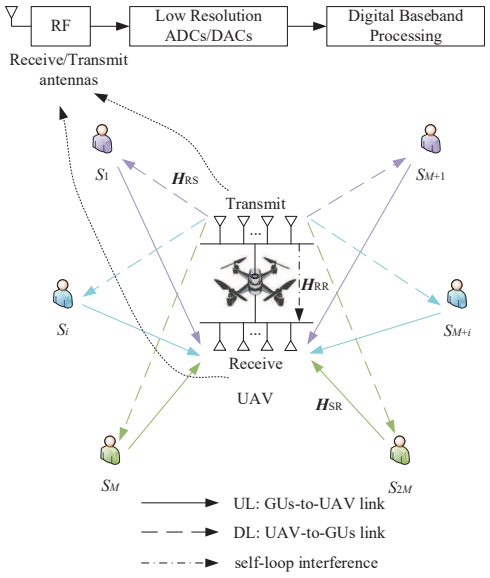

Fig. 1. UAV-enabled massive MIMO-NOMA FD TWR system with low-resolution ADCs/DACs.

Notation: The matrices, vectors, and variables are represented in bold capital, bold lowercase, and italics letters, respectively. $\mathbb{C}^{p\times q}$ denotes a complex matrix of dimension $p \times q$, $\boldsymbol{I}_r$ denotes an $r \times r$ identity matrix, and $\mathrm{diag}\,(\cdot)$ is a diagonal matrix. Moreover, $(\cdot)^{\mathrm{H}}$, $(\cdot)^*$, $(\cdot)^{\mathrm{T}}$, and $(\cdot)^{-1}$ stand for the conjugate-transpose, the conjugate, the transpose, and the inverse of a matrix, respectively, while $\|\cdot\|$ denotes the Euclidian norm of a vector, and $\|\cdot\|_{\mathrm{F}}$ is the Frobenius norm of a matrix. Also, the operations of expectation, variance, trace and scalar quantization are denoted by $\mathbb{E}\{\cdot\}$, $\mathbb{V}\mathrm{ar}\{\cdot\}$, $\mathrm{Tr}\,(\cdot)$, $\mathbb{Q}\,(\cdot)$, respectively. Finally, $\mathcal{CN}\,(a,b)$ represents a circularly symmetric complex Gaussian distribution with mean of a and variance of b.

II. System Model

As shown in Fig. 1, we consider a multi-pair massive MIMO-NOMA system that consists of M pairs of ground users (GU), and a two-way shared AF FD UAV relay (UR). The ith GU $S_i, i = 1, 2, \ldots, M$ exchanges information with the $(M + i)$th GU S_{M+i} on the same time-frequency resources via UR, since there is no available direct link between them due to the deep shadowing and/or obstacle. We assume that UR is deployed at a fixed altitude and equipped with N transmit antennas and N receive antennas, while each GU has a single transmit/receive antenna. Besides, both the UL and DL RF chains of UR employ low-resolution ADCs/DACs to save the cost and energy. The low-resolution ADCs cause quantization

TABLE I
LITERATURE SURVEY

Ref./Prop.	Rician Channel	Channel Estimation with Impact of Quantization Error	Two-Way NOMA Transmission	Hardware Impairment	Performance Index
[17]	×	×	×	Low-resolution ADCs	SE
[18]	×	✓	×	Low-resolution ADCs	ASR
[19]	✓	×	×	Low-resolution ADCs	ASR
[20]	✓	×	×	Low-resolution ADCs	SE, EE
[21]	✓	×	×	Low-resolution ADCs/DACs	UL/DL rate
[22]	✓	×	×	Low-resolution ADCs/DACs	UL/DL rate, EE
prop.	✓	✓	✓	Low-resolution ADCs/DACs	SE, EE

errors in the channel estimation and UL data reception phases, while the low-resolution DACs introduce signal distortion for the DL data transmission [22]. Therefore, the studied system is double quantized. Without loss of generality, a 3D Cartesian coordinate system is considered. The location of S_i is assumed to be fixed at $\boldsymbol{q}_i = [x_{S_i}, y_{S_i}, 0]^{\mathrm{T}}$, and UR's position is set to $\boldsymbol{u} = [x_{\mathrm{U}}, y_{\mathrm{U}}, H]^{\mathrm{T}}$, thereby the distance between S_i and UR is given as $d_i = \|\boldsymbol{u} - \boldsymbol{q}_i\|$. We define the vectors $\boldsymbol{h}_{\mathrm{SR},i} \in \mathbb{C}^{N\times 1}$ and $\boldsymbol{h}_{\mathrm{RS},i}^{\mathrm{T}} \in \mathbb{C}^{1\times N}$ as the channels from S_i to UR and UR to S_i, respectively. For $X \in \{\mathrm{SR},\mathrm{RS}\}$, $\boldsymbol{h}_{X,i}$ can be modeled as

$$\boldsymbol{h}_{X,i} = \sqrt{\frac{\beta_0 \left(\mathrm{Pr}_i^{\mathrm{L}} \eta_{\mathrm{L}} + \mathrm{Pr}_i^{\mathrm{NL}} \eta_{\mathrm{NL}}\right) K_{X,i}}{d_i^k \left(K_{X,i}+1\right)}} \bar{\boldsymbol{g}}_{X,i} + \sqrt{\frac{\beta_0 \left(\mathrm{Pr}_i^{\mathrm{L}} \eta_{\mathrm{L}} + \mathrm{Pr}_i^{\mathrm{NL}} \eta_{\mathrm{NL}}\right)}{d_i^k \left(K_{X,i}+1\right)}} \tilde{\boldsymbol{g}}_{X,i}, \tag{1}$$

where β_0 represents the channel power gain constant at the reference distance of 1 meter, while $\mathrm{Pr}_i^{\mathrm{L}}$ and $\mathrm{Pr}_i^{\mathrm{NL}}$ denote the LoS and NLoS probability between S_i and UR, respectively, whose expressions are refer to [23] (Eq.((3) and (5))[1]. η_{L} and η_{NL} are the additional attenuation factors for the LoS and NLoS links, respectively, and k is the path loss exponent. In addition, $K_{X,i}$ represents the Rician factor of S_i, $\bar{\boldsymbol{g}}_{X,i}$ denotes the deterministic direct component, and $\tilde{\boldsymbol{g}}_{X,i}$ denotes the random scattering component, which consists of independent and identically distributed (*i.i.d.*) $\mathcal{CN}(0,1)$ elements. We assume that the UAV antennas are the uniform linear arrays, then, $\bar{\boldsymbol{g}}_{X,i}$ can be expressed as

$$\bar{\boldsymbol{g}}_{X,i} = \left[1, e^{j(2\pi l/\lambda)\sin(\theta_i)}, \ldots, e^{j(N-1)(2\pi l/\lambda)\sin(\theta_i)}\right]^{\mathrm{T}}, \tag{2}$$

where λ represents the carrier wavelength, l denotes the antenna spacing, and θ_i denotes the angle of arrival from S_i to UR. For convenience, we concatenate the channel vectors $\boldsymbol{h}_{\mathrm{SR},i}$ and $\boldsymbol{h}_{\mathrm{RS},i}^{\mathrm{T}}$ to obtain the channels in matrix form as $\boldsymbol{H}_{\mathrm{SR}} = [\boldsymbol{h}_{\mathrm{SR},1}, \boldsymbol{h}_{\mathrm{SR},2}, ..., \boldsymbol{h}_{\mathrm{SR},2M}] \in \mathbb{C}^{N\times 2M}$ and $\boldsymbol{H}_{\mathrm{RS}}^{\mathrm{T}} = [\boldsymbol{h}_{\mathrm{RS},1}, \boldsymbol{h}_{\mathrm{RS},2}, ..., \boldsymbol{h}_{\mathrm{RS},2M}]^{\mathrm{T}} \in \mathbb{C}^{2M\times N}$. Additionally, the residual self-loop interference (RSI) channel matrix obtained by self-interference cancellation [24], [25] at UR is denoted by $\boldsymbol{H}_{\mathrm{RR}} \in \mathbb{C}^{N\times N}$, which is distributed as $\mathcal{CN}\left(\boldsymbol{0}, \sigma_{\mathrm{RR}}^2 \boldsymbol{I}_N\right)$. The imperfect CSI is assumed for both UL and DL channels, and the minimum mean squared error (MMSE) channel estimation process is provided in the next sub-section.

[1] $\mathrm{Pr}_i^{\mathrm{L}} = \left[1 + c_1 e^{-c_2(\vartheta_i - c_1)}\right]^{-1}$, $\vartheta_i = \frac{180^\circ}{\pi}\arcsin\left(H/d_i\right)$ and $\mathrm{Pr}_i^{\mathrm{NL}} = 1 - \mathrm{Pr}_i^{\mathrm{L}}$, where c_1 and c_2 are parameters related to the communication environment.

A. Channel Estimation with The Impact of ADCs/DACs

By convention of massive MIMO analysis, we assume that channel estimation is performed by pilot sounding [20]. During each coherence interval T (in symbols), the M GU pairs simultaneously transmit their mutually orthogonal pilot sequences of τ symbols to UR for the channel estimation. Thus, the received signals at the receive and transmit antenna arrays of UR are given by

$$\boldsymbol{Y}_{\mathrm{rp}} = \sum_{i=1}^{2M} \sqrt{\alpha_{\boldsymbol{\Phi},i} P_{\boldsymbol{\Phi}}} \boldsymbol{h}_{\mathrm{SR},i} \boldsymbol{\phi}_i + \boldsymbol{N}_{\mathrm{rp}} = \sqrt{P_{\boldsymbol{\Phi}}} \boldsymbol{H}_{\mathrm{SR}} \sqrt{\boldsymbol{A}_{\boldsymbol{\Phi}}} \boldsymbol{\Phi} + \boldsymbol{N}_{\mathrm{rp}}, \tag{3}$$

$$\boldsymbol{Y}_{\mathrm{tp}} = \sum_{i=1}^{2M} \sqrt{\alpha_{\boldsymbol{\Phi},i} P_{\boldsymbol{\Phi}}} \boldsymbol{h}_{\mathrm{RS},i} \boldsymbol{\phi}_i + \boldsymbol{N}_{\mathrm{tp}} = \sqrt{P_{\boldsymbol{\Phi}}} \boldsymbol{H}_{\mathrm{RS}} \sqrt{\boldsymbol{A}_{\boldsymbol{\Phi}}} \boldsymbol{\Phi} + \boldsymbol{N}_{\mathrm{tp}}, \tag{4}$$

respectively, where $P_{\boldsymbol{\Phi}}$ is the transmit power of pilot symbols, $A_{\boldsymbol{\Phi}} \in \mathbb{C}^{2M\times 2M}$ is the power scaling coefficient matrix whose ith diagonal element is $\alpha_{\boldsymbol{\Phi},i}$, while $\boldsymbol{\Phi} \in \mathbb{C}^{2M\times\tau}$ is the pilot matrix whose ith row is $\boldsymbol{\phi}_i$, satisfying $\boldsymbol{\Phi}\boldsymbol{\Phi}^{\mathrm{H}} = \boldsymbol{I}_{2M}$. Also, $\boldsymbol{N}_{\mathrm{rp}} \in \mathbb{C}^{N\times\tau}$ and $\boldsymbol{N}_{\mathrm{tp}} \in \mathbb{C}^{N\times\tau}$ are the additive white Gaussian noise (AWGN) matrix including *i.i.d.* $\mathcal{CN}(0,1)$ elements.

We adopt the additive quantization noise model (AQNM) for tractable analysis, and the quantized signals at UR's receive and transmit antenna arrays can be expressed as

$$\bar{\boldsymbol{Y}}_{\mathrm{rp}} = \mathbb{Q}\left\{\boldsymbol{Y}_{\mathrm{rp}}\right\} = \alpha_r \boldsymbol{Y}_{\mathrm{rp}} + \boldsymbol{N}_{\mathrm{rq}}, \tag{5}$$

$$\bar{\boldsymbol{Y}}_{\mathrm{tp}} = \mathbb{Q}\left\{\boldsymbol{Y}_{\mathrm{tp}}\right\} = \alpha_t \boldsymbol{Y}_{\mathrm{tp}} + \boldsymbol{N}_{\mathrm{tq}}, \tag{6}$$

respectively, where $\alpha_r = 1-\rho$, $\alpha_t = 1-\rho$ represent the low-resolution distortion factors, and the values of ρ for different quantization bits b can be found in [26]. $\boldsymbol{N}_{\mathrm{rq}} \in \mathbb{C}^{N\times\tau}$ and $\boldsymbol{N}_{\mathrm{tq}} \in \mathbb{C}^{N\times\tau}$ are quantization noises with covariance matrix $\boldsymbol{R}_{\boldsymbol{N}_{\mathrm{rq}}} = \alpha_r\left(1-\alpha_r\right)\mathrm{diag}\left(P_{\boldsymbol{\Phi}}\boldsymbol{H}_{\mathrm{SR}}\boldsymbol{A}_{\boldsymbol{\Phi}}\boldsymbol{H}_{\mathrm{SR}}^{\mathrm{H}} + \boldsymbol{I}_N\right)$, $\boldsymbol{R}_{\boldsymbol{N}_{\mathrm{tq}}} = \alpha_t\left(1-\alpha_t\right)\mathrm{diag}\left(P_{\boldsymbol{\Phi}}\boldsymbol{H}_{\mathrm{RS}}\boldsymbol{A}_{\boldsymbol{\Phi}}\boldsymbol{H}_{\mathrm{RS}}^{\mathrm{H}} + \boldsymbol{I}_N\right)$, respectively.

We assumed that UR employs the linear MMSE estimator to estimate the channel matrices $\boldsymbol{H}_{\mathrm{SR}}$ and $\boldsymbol{H}_{\mathrm{RS}}$, Then, according to the orthogonality principle of MMSE criterion, there are

$$\boldsymbol{h}_{\mathrm{SR},i} = \hat{\boldsymbol{h}}_{\mathrm{SR},i} + \boldsymbol{e}_{\mathrm{SR},i}, \tag{7}$$

$$\boldsymbol{h}_{\mathrm{RS},i} = \hat{\boldsymbol{h}}_{\mathrm{RS},i} + \boldsymbol{e}_{\mathrm{RS},i}, \tag{8}$$

respectively, where $\hat{\boldsymbol{h}}_{\mathrm{SR},i}$, $\hat{\boldsymbol{h}}_{\mathrm{RS},i}$, $\boldsymbol{e}_{\mathrm{SR},i}$ and $\boldsymbol{e}_{\mathrm{RS},i}$ are the ith columns of the estimated matrices $\hat{\boldsymbol{H}}_{\mathrm{SR}}$, $\hat{\boldsymbol{H}}_{\mathrm{RS}}$, and the estimation error matrices $\boldsymbol{\Xi}_{\mathrm{SR}}$, $\boldsymbol{\Xi}_{\mathrm{RS}}$, respectively, which are independent of each other.

The distributions of the above channels are given in ***Lemma 1***, which are necessary for the subsequent analysis.

Lemma 1: The elements of $\hat{\boldsymbol{h}}_{\mathrm{SR},i}$, $\hat{\boldsymbol{h}}_{\mathrm{RS},i}$, $\boldsymbol{e}_{\mathrm{SR},i}$ and $\boldsymbol{e}_{\mathrm{RS},i}$ are independent Gaussian random variables with zero mean and variance $\delta_{\mathrm{SR},i}$, $\delta_{\mathrm{RS},i}$, $\varsigma_{\mathrm{SR},i}$ and $\varsigma_{\mathrm{RS},i}$, respectively, which can be given as

$$\delta_{\mathrm{SR},i}=\frac{\beta_{\mathrm{SR},i}\left(K_{\mathrm{SR},i}+\Psi_{\mathrm{SR},i}\right)}{1+K_{\mathrm{SR},i}} \text{ with } \Psi_{\mathrm{SR},i}=\frac{\alpha_r\alpha_{\boldsymbol{\Phi},i}P_{\boldsymbol{\Phi}}\beta_{\mathrm{SR},i}}{1+\alpha_{\boldsymbol{\Phi},i}P_{\boldsymbol{\Phi}}\beta_{\mathrm{SR},i}},$$
$$\delta_{\mathrm{RS},i}=\frac{\beta_{\mathrm{RS},i}\left(K_{\mathrm{RS},i}+\Psi_{\mathrm{RS},i}\right)}{1+K_{\mathrm{RS},i}} \text{ with } \Psi_{\mathrm{RS},i}=\frac{\alpha_t\alpha_{\boldsymbol{\Phi},i}P_{\boldsymbol{\Phi}}\beta_{\mathrm{RS},i}}{1+\alpha_{\boldsymbol{\Phi},i}P_{\boldsymbol{\Phi}}\beta_{\mathrm{RS},i}},$$
$$\varsigma_{\mathrm{SR},i}=\frac{\beta_{\mathrm{SR},i}+(1-\alpha_r)\alpha_{\boldsymbol{\Phi},i}P_{\boldsymbol{\Phi}}\beta_{\mathrm{SR},i}^2}{\left(1+K_{\mathrm{SR},i}\right)\left(1+\alpha_{\boldsymbol{\Phi},i}P_{\boldsymbol{\Phi}}\beta_{\mathrm{SR},i}\right)},$$
$$\varsigma_{\mathrm{RS},i}=\frac{\beta_{\mathrm{RS},i}+(1-\alpha_t)\alpha_{\boldsymbol{\Phi},i}P_{\boldsymbol{\Phi}}\beta_{\mathrm{RS},i}^2}{\left(1+K_{\mathrm{RS},i}\right)\left(1+\alpha_{\boldsymbol{\Phi},i}P_{\boldsymbol{\Phi}}\beta_{\mathrm{RS},i}\right)},$$

where $\beta_{X,i}=\left[\beta_0\left(\mathrm{Pr}_i^{\mathrm{L}}\eta_{\mathrm{L}}+\mathrm{Pr}_i^{\mathrm{NL}}\eta_{\mathrm{NL}}\right)\right]/d_i^k$, $X\in\{\mathrm{SR},\mathrm{RS}\}$.

Proof: Refer to Appendix A.

B. Data Transmission of Double Quantized System

At the uth time instant of the data transmission interval, all GUs transmit superimposed signal by invoking SC to UR, and UR broadcasts the signal to all GUs. Thus, the received signals at UR and the mth GU S_m are given by

$$\boldsymbol{y}_{\mathrm{R}}(u)=\sum_{i=1}^{2M}\sqrt{\varrho_i P_{\mathrm{S}}}\boldsymbol{h}_{\mathrm{SR},i}x_i(u)+\boldsymbol{H}_{\mathrm{RR}}\tilde{\boldsymbol{t}}_{\mathrm{R}}(u)+\boldsymbol{n}_{\mathrm{R}}(u), \quad (9)$$

$$y_m(u)=\boldsymbol{h}_{\mathrm{RS},m}^{\mathrm{T}}\boldsymbol{F}\boldsymbol{y}_{\mathrm{R}}(u-\ell)+n_m(u), \quad (10)$$

respectively, where x_i denotes the transmitted signal for S_i that satisfies $\mathbb{E}\{|x_i|^2\}=1$, P_{S} is the GUs' transmit power, ϱ_i is the power allocation coefficient of S_i. To facilitate NOMA transmission, we assumed that the UAV-to-GU channels satisfy $|h_{X,1}|^2>|h_{X,2}|^2>\ldots>|h_{X,2M}|^2$ ($X\in\{\mathrm{SR},\mathrm{RS}\}$), thus, we have $\varrho_1>\varrho_2>\ldots>\varrho_{2M}$ and $\varrho_1+\varrho_2+\ldots+\varrho_{2M}=1$. Furthermore, $\tilde{\boldsymbol{t}}_{\mathrm{R}}$ and $\boldsymbol{n}_{\mathrm{R}}$ denote the RSI signal and the AWGN at UR, respectively, $\tilde{\boldsymbol{t}}_{\mathrm{R}}$ is limited by $\mathbb{E}\{\tilde{\boldsymbol{t}}_{\mathrm{R}}\tilde{\boldsymbol{t}}_{\mathrm{R}}^{\mathrm{H}}\}=(P_{\mathrm{R}}/N)\boldsymbol{I}_N$, where P_{R} is the transmitted power of UR, and $\boldsymbol{n}_{\mathrm{R}}$ consists of *i.i.d.* $\mathcal{CN}(0,\sigma_{\mathrm{R}}^2)$ elements. Additionally, $\boldsymbol{F}$ denotes the precoder matrix, which will discuss in the next sub-section, ℓ is the processing delay due to the FD transmission of UR, and n_m is the AWGN of S_m with $n_m\sim\mathcal{CN}(0,\sigma_m^2)$.

After low-resolution ADCs/DACs, the received signals in (9) and (10) become

$$\boldsymbol{y}_{\mathrm{R}}^{\mathrm{q}}=\mathbb{Q}(\boldsymbol{y}_{\mathrm{R}})=\alpha_r\sum_{i=1}^{2M}\sqrt{\varrho_i P_{\mathrm{S}}}\boldsymbol{h}_{\mathrm{SR},i}x_i+\alpha_r\boldsymbol{H}_{\mathrm{RR}}\tilde{\boldsymbol{t}}_{\mathrm{R}}+\alpha_r\boldsymbol{n}_{\mathrm{R}}+\boldsymbol{n}_{\mathrm{rq}}, \quad (11)$$

$$\boldsymbol{y}_m^{\mathrm{q}}=\mathbb{Q}(\boldsymbol{y}_m)=\alpha_r\alpha_t\boldsymbol{h}_{\mathrm{RS},m}^{\mathrm{T}}\boldsymbol{F}\left(\sum_{i=1}^{2M}\sqrt{\varrho_i P_{\mathrm{S}}}\boldsymbol{h}_{\mathrm{SR},i}x_i+\boldsymbol{H}_{\mathrm{RR}}\tilde{\boldsymbol{t}}_{\mathrm{R}}+\boldsymbol{n}_{\mathrm{R}}\right)+\alpha_t\boldsymbol{h}_{\mathrm{RS},m}^{\mathrm{T}}\boldsymbol{F}\boldsymbol{n}_{\mathrm{rq}}+\boldsymbol{h}_{\mathrm{RS},m}^{\mathrm{T}}\boldsymbol{n}_{\mathrm{tq}}+n_m, \quad (12)$$

respectively, where the time labels are dropped for the sake of brevity, which are also removed in the sequel. In addition, $\boldsymbol{n}_{\mathrm{rq}}$ and $\boldsymbol{n}_{\mathrm{tq}}$ are the additive ADC and DAC quantization noise with covariance matrix $\boldsymbol{R}_{\boldsymbol{n}_{\mathrm{rq}}}=\alpha_r(1-\alpha_r)\,\mathrm{diag}\left(P_{\mathrm{S}}\boldsymbol{H}_{\mathrm{SR}}\boldsymbol{\varrho}\boldsymbol{H}_{\mathrm{SR}}^{\mathrm{H}}+(P_{\mathrm{R}}/N)\boldsymbol{I}_N+\sigma_{\mathrm{R}}^2\boldsymbol{I}_N\right)$ and $\boldsymbol{R}_{\boldsymbol{n}_{\mathrm{tq}}}=\alpha_t(1-\alpha_t)(P_{\mathrm{R}}/N)$, respectively, where $\boldsymbol{\varrho}\triangleq\mathrm{diag}(\varrho_1,\varrho_2,...,\varrho_{2M})$.

We consider that use $(m,\hat{m})$ to denote the GU pair S_m and $S_{\hat{m}}$ that wish to exchange information with each other, where $\hat{m}=\begin{cases}M+m, & m\le M\\ m-M, & \text{otherwise}\end{cases}$, $m=1,2,\ldots,2M$. Then, using NOMA[2] and considering imperfect SIC, $\boldsymbol{y}_m^{\mathrm{q}}$ in (12) becomes

$$\bar{\boldsymbol{y}}_m^{\mathrm{q}}=\alpha_r\alpha_t\boldsymbol{h}_{\mathrm{RS},m}^{\mathrm{T}}\boldsymbol{F}\Bigg(\boldsymbol{H}_{\mathrm{RR}}\tilde{\boldsymbol{t}}_{\mathrm{R}}+\boldsymbol{n}_{\mathrm{R}}+\sum_{\substack{i=1\\ i\neq m}}^{\hat{m}-1}\sqrt{\varpi\varrho_i P_{\mathrm{S}}}\boldsymbol{h}_{\mathrm{SR},i}x_i+\sum_{\substack{i=\hat{m}\\ i\neq m}}^{2M}\sqrt{\varrho_i P_{\mathrm{S}}}\boldsymbol{h}_{\mathrm{SR},i}x_i\Bigg)+\alpha_r\alpha_t\boldsymbol{\kappa}_m\sqrt{\varrho_m P_{\mathrm{S}}}x_m + \alpha_t\boldsymbol{h}_{\mathrm{RS},m}^{\mathrm{T}}\boldsymbol{F}\boldsymbol{n}_{\mathrm{rq}}+\boldsymbol{h}_{\mathrm{RS},m}^{\mathrm{T}}\boldsymbol{n}_{\mathrm{tq}}+n_m, \quad (13)$$

where $\sqrt{\varpi}$ is the proportion of residual signals caused by imperfect SIC, and $\boldsymbol{\kappa}_m\triangleq\boldsymbol{h}_{\mathrm{RS},m}^{\mathrm{T}}\boldsymbol{F}\boldsymbol{h}_{\mathrm{SR},m}-\hat{\boldsymbol{h}}_{\mathrm{RS},m}^{\mathrm{T}}\boldsymbol{F}\hat{\boldsymbol{h}}_{\mathrm{SR},m}$ denotes the RSI after S_m performs imperfect self-interference cancellation to eliminate its own transmit signal x_m[3].

C. Precoder Design

The MRC/MRT precoder matrix $\boldsymbol{F}$ using the estimated channel can be formulated as

$$\boldsymbol{F}\triangleq\varepsilon\boldsymbol{W}=\varepsilon\hat{\boldsymbol{H}}_{\mathrm{RS}}^{*}\boldsymbol{\Lambda}\hat{\boldsymbol{H}}_{\mathrm{SR}}^{\mathrm{H}}=\varepsilon\sum_{i=1}^{2M}\left(\hat{\boldsymbol{h}}_{\mathrm{RS},i}^{*}\hat{\boldsymbol{h}}_{\mathrm{SR},\hat{i}}^{\mathrm{H}}\right), \quad (14)$$

where the block-diagonal matrix is given as $\boldsymbol{\Lambda}=[\boldsymbol{\Lambda}_1,\boldsymbol{\Lambda}_2;\boldsymbol{\Lambda}_2,\boldsymbol{\Lambda}_1]$ with $\boldsymbol{\Lambda}_1=\boldsymbol{0}\in\mathbb{C}^{M\times M}$, $\boldsymbol{\Lambda}_2=\boldsymbol{I}_M$, and ε is the amplification factor, which is given in (15) at the top of the next page.

III. Performance Analysis

In this section, we derive a closed form approximation of the sum SE. To gain more useful insights, the asymptotic results and the power scaling schemes are also discussed.

A. Spectrum Efficiency Analysis

To study the system SE, we first deduce the signal-to-interference-noise ratio (SINR) for decoding $x_{\hat{m}}$ at S_m. The received signal at S_m used to detect its desired signal $x_{\hat{m}}$ is given by (16) at the top of this page. From (16), we can see that the detected signal includes the following seven components: i) desired signal; ii) detection uncertainty; iii) inter-pair interference caused by other GU pairs after SIC;

[2]If the S_m intends to decode the signal of $S_{\hat{m}}$ correctly, it needs to successfully and continuously decode the previous signals of $\hat{m}$ GUs, and then utilizes SIC to eliminate the interference for all GUs i, when $i<\hat{m}$, while the signals for all other GUs with $i>\hat{m}$ will be regarded as noise.

[3]Each GU S_m is assumed to be fully aware of the estimated UL/DL channels and its own signal x_m, and performs self-interference cancellation before decoding the expected signal $x_{\hat{m}}$. In this paper, we consider that the self-interference cancellation is imperfect, i.e., there exists RSI, which is denoted by $\boldsymbol{\kappa}_m$.

$$\varepsilon = \sqrt{\frac{P_{\mathrm{R}}}{\alpha_r^2 P_{\mathrm{S}} \mathbb{E}\left\{\left\|\boldsymbol{W}\boldsymbol{H}_{\mathrm{SR}}\boldsymbol{\varrho}^{\frac{1}{2}}\right\|_{\mathrm{F}}^2\right\} + \frac{\alpha_r^2 P_{\mathrm{R}}}{N}\mathbb{E}\left\{\left\|\boldsymbol{W}\boldsymbol{H}_{\mathrm{RR}}\right\|_{\mathrm{F}}^2\right\} + \alpha_r^2\sigma_{\mathrm{R}}^2\mathbb{E}\left\{\left\|\boldsymbol{W}\right\|_{\mathrm{F}}^2\right\} + \mathbb{E}\left\{\left\|\boldsymbol{W}\boldsymbol{R}_{\boldsymbol{n}_{\mathrm{rq}}}^{\frac{1}{2}}\right\|_{\mathrm{F}}^2\right\}}} \tag{15}$$

$$\begin{aligned}\bar{\boldsymbol{y}}_{m,\hat{m}}^{\mathrm{q}} = {} & \underbrace{\alpha_r\alpha_t\sqrt{\varrho_{\hat{m}}P_{\mathrm{S}}}\mathbb{E}\left\{\boldsymbol{h}_{\mathrm{RS},m}^{\mathrm{T}}\boldsymbol{F}\boldsymbol{h}_{\mathrm{SR},\hat{m}}\right\}x_{\hat{m}}}_{\text{desired signal}} + \underbrace{\alpha_r\alpha_t\sqrt{\varrho_{\hat{m}}P_{\mathrm{S}}}\left(\boldsymbol{h}_{\mathrm{RS},m}^{\mathrm{T}}\boldsymbol{F}\boldsymbol{h}_{\mathrm{SR},\hat{m}} - \mathbb{E}\left\{\boldsymbol{h}_{\mathrm{RS},m}^{\mathrm{T}}\boldsymbol{F}\boldsymbol{h}_{\mathrm{SR},\hat{m}}\right\}\right)x_{\hat{m}}}_{\text{detection uncertainty}} \\ & \underbrace{+\alpha_r\alpha_t\sum_{\substack{i=1\\ i\neq m}}^{\hat{m}-1}\sqrt{\varpi\varrho_i P_{\mathrm{S}}}\boldsymbol{h}_{\mathrm{RS},m}^{\mathrm{T}}\boldsymbol{F}\boldsymbol{h}_{\mathrm{SR},i}x_i + \alpha_r\alpha_t\sum_{\substack{i=\hat{m}+1\\ i\neq m}}^{2M}\sqrt{\varrho_i P_{\mathrm{S}}}\boldsymbol{h}_{\mathrm{RS},m}^{\mathrm{T}}\boldsymbol{F}\boldsymbol{h}_{\mathrm{SR},i}x_i}_{\text{inter-pair interference caused by other GU pairs after SIC}} + \underbrace{\alpha_r\alpha_t\sqrt{\varrho_m P_{\mathrm{S}}}\boldsymbol{\kappa}_m x_m}_{\text{RSI at } S_m} \\ & \underbrace{+\alpha_r\alpha_t\boldsymbol{h}_{\mathrm{RS},m}^{\mathrm{T}}\boldsymbol{F}\boldsymbol{H}_{\mathrm{RR}}\tilde{\boldsymbol{t}}_{\mathrm{R}}}_{\text{amplified RSI at UR}} + \underbrace{\alpha_t\boldsymbol{h}_{\mathrm{RS},m}^{\mathrm{T}}\boldsymbol{F}\boldsymbol{n}_{\mathrm{rq}}}_{\text{quantization noise of ADCs}} + \underbrace{\boldsymbol{h}_{\mathrm{RS},m}^{\mathrm{T}}\boldsymbol{n}_{\mathrm{tq}}}_{\text{quantization noise of DACs}} + \underbrace{\alpha_r\alpha_t\boldsymbol{h}_{\mathrm{RS},m}^{\mathrm{T}}\boldsymbol{F}\boldsymbol{n}_{\mathrm{R}}}_{\text{amplified noise at UR}} + \underbrace{n_m}_{\text{AWGN at } S_m} \\ & \underbrace{\qquad\qquad\qquad\qquad\qquad\qquad\qquad\qquad\qquad\qquad}_{\text{quantization noise from low-resolution converters}} \qquad \underbrace{\qquad\qquad\qquad\qquad\qquad\qquad\qquad\qquad}_{\text{compound noise}}\end{aligned} \tag{16}$$

iv) RSI at GU; v) amplified RSI at the UR; vi) quantization noise from low-resolution converters; and vii) compound noise consisting of amplified noise at the UR and AWGN at GU. Therefore, the SINR is expressed as

$$\gamma_{m,\hat{m}} = \frac{\alpha_r^2\alpha_t^2\varrho_{\hat{m}}P_{\mathrm{S}}\left|\mathbb{E}\left\{\boldsymbol{h}_{\mathrm{RS},m}^{\mathrm{T}}\boldsymbol{F}\boldsymbol{h}_{\mathrm{SR},\hat{m}}\right\}\right|^2}{L_{1_{m,\hat{m}}}+L_{2_{m,\hat{m}}}+L_{3_{m,\hat{m}}}+L_{4_{m,\hat{m}}}+L_{5_{m,\hat{m}}}+L_{6_{m,\hat{m}}}}, \tag{17}$$

where $L_{1_{m,\hat{m}}}$, $L_{2_{m,\hat{m}}}$, $L_{3_{m,\hat{m}}}$, $L_{4_{m,\hat{m}}}$, $L_{5_{m,\hat{m}}}$ and $L_{6_{m,\hat{m}}}$ in (17) corresponds to ii), iii), iv), v), vi) and vii) in (16), respectively, which can be given as

$$\begin{aligned}L_{1_{m,\hat{m}}} &= \alpha_r^2\alpha_t^2\varrho_{\hat{m}}P_{\mathrm{S}}\mathbb{V}\mathrm{ar}\left(\boldsymbol{h}_{\mathrm{RS},m}^{\mathrm{T}}\boldsymbol{F}\boldsymbol{h}_{\mathrm{SR},\hat{m}}\right), \\ L_{2_{m,\hat{m}}} &= \varpi\alpha_r^2\alpha_t^2P_{\mathrm{S}}\sum_{i=1,\neq m}^{\hat{m}-1}\varrho_i\mathbb{E}\left\{\left|\boldsymbol{h}_{\mathrm{RS},m}^{\mathrm{T}}\boldsymbol{F}\boldsymbol{h}_{\mathrm{SR},i}\right|^2\right\} \\ &\quad + \alpha_r^2\alpha_t^2P_{\mathrm{S}}\sum_{i=\hat{m}+1,i\neq m}^{2M}\varrho_i\mathbb{E}\left\{\left|\boldsymbol{h}_{\mathrm{RS},m}^{\mathrm{T}}\boldsymbol{F}\boldsymbol{h}_{\mathrm{SR},i}\right|^2\right\}, \\ L_{3_{m,\hat{m}}} &= \alpha_r^2\alpha_t^2\varrho_m P_{\mathrm{S}}\mathbb{E}\left\{\left|\boldsymbol{\kappa}_m\right|^2\right\}, \\ L_{4_{m,\hat{m}}} &= \frac{\alpha_r^2\alpha_t^2P_{\mathrm{R}}}{N}\mathbb{E}\left\{\left\|\boldsymbol{h}_{\mathrm{RS},m}^{\mathrm{T}}\boldsymbol{F}\boldsymbol{H}_{\mathrm{RR}}\right\|^2\right\}, \\ L_{5_{m,\hat{m}}} &= \alpha_t^2\mathbb{E}\left\{\left\|\boldsymbol{h}_{\mathrm{RS},m}^{\mathrm{T}}\boldsymbol{F}\boldsymbol{n}_{\mathrm{rq}}\right\|^2\right\} + \mathbb{E}\left\{\left\|\boldsymbol{h}_{\mathrm{RS},m}^{\mathrm{T}}\boldsymbol{n}_{\mathrm{tq}}\right\|^2\right\}, \\ L_{6_{m,\hat{m}}} &= \alpha_r^2\alpha_t^2\sigma_{\mathrm{R}}^2\mathbb{E}\left\{\left\|\boldsymbol{h}_{\mathrm{RS},m}^{\mathrm{T}}\boldsymbol{F}\right\|^2\right\} + \sigma_m^2.\end{aligned}$$

Based on (17), the sum SE of the system can be given as

$$R_{\mathrm{SE}} = \frac{T-\tau}{T}\sum_{m=1}^{2M}\log_2\left(1+\gamma_{m,\hat{m}}\right). \tag{18}$$

The closed-form expression of R_{SE} in (18) can be obtained by using random matrix theory, as shown in Theorem 1.

Theorem 1: For an UAV-enabled massive MIMO-NOMA FD TWR system with imperfect CSI, imperfect SIC, and low-resolution ADCs/DACs, the closed approximation form of the sum SE can be expressed as

$$R_{\mathrm{SE}} = \frac{T-\tau}{T}\sum_{m=1}^{2M}\log_2\left(1+\frac{N^4\varrho_{\hat{m}}P_{\mathrm{S}}\delta_{\mathrm{RS},m}^2\delta_{\mathrm{SR},\hat{m}}^2}{\Delta_1+\Delta_2+\Delta_3+\Delta_4+\Delta_5}\right), \tag{19}$$

where

$$\begin{aligned}\Delta_1 &= \varpi\sum_{i=1,i\neq m}^{\hat{m}-1}\sum_{j=1}^{2M}\varrho_i P_{\mathrm{S}}\psi_{\mathrm{RS},mj}\psi_{\mathrm{SR},\hat{j}i} - N^4\varrho_{\hat{m}}P_{\mathrm{S}} \\ &\quad\times\delta_{\mathrm{RS},m}^2\delta_{\mathrm{SR},\hat{m}}^2 + \sum_{i=\hat{m},i\neq m}^{2M}\sum_{j=1}^{2M}\varrho_i P_{\mathrm{S}}\psi_{\mathrm{RS},mj}\psi_{\mathrm{SR},\hat{j}i}, \\ \Delta_2 &= \left[P_{\mathrm{S}}\left(\varpi\sum_{i=1,i\neq m}^{\hat{m}-1}\upsilon_{1_i}+\upsilon_{1_m}+\sum_{i=\hat{m},i\neq m}^{2M}\upsilon_{1_i}\right)+\Theta\right] \\ &\quad\times\left[N(\delta_{\mathrm{SR},\hat{m}}\psi_{\mathrm{RS},mm}+\delta_{\mathrm{SR},m}\psi_{\mathrm{RS},m\hat{m}})+\Omega\varsigma_{\mathrm{RS},m}\right], \\ \Delta_3 &= N\varsigma_{\mathrm{RS},m}P_{\mathrm{S}}\left(\varpi\sum_{i=1,i\neq m}^{\hat{m}-1}\upsilon_{2_i}+\upsilon_{2_m}+\sum_{i=\hat{m},i\neq m}^{2M}\upsilon_{2_i}\right), \\ \Delta_4 &= J_m\left(\Omega P_{\mathrm{S}}\sum_{i=1}^{2M}\upsilon_{1_i}+\Omega\Theta+N^3P_{\mathrm{S}}\sum_{i=1}^{2M}\varrho_i\delta_{\mathrm{RS},i}\delta_{\mathrm{SR},\hat{i}}^2\right), \\ \Delta_5 &= N\sum_{i=1}^{2M}\psi_{\mathrm{RS},im}\upsilon_{3_{\hat{i}}}+N^2\left(J_m+\varsigma_{\mathrm{RS},m}\right)\sum_{i=1}^{2M}\delta_{\mathrm{RS},i}\upsilon_{3_i},\end{aligned}$$

where $\Omega = N^2\sum_{i=1}^{2M}\delta_{\mathrm{RS},i}\delta_{\mathrm{SR},\hat{i}}$, $\Theta = P_{\mathrm{R}}\sigma_{\mathrm{RR}}^2 + \sigma_{\mathrm{R}}^2$, $J_m = \left(\alpha_t^{-1}-1\right)\left(\delta_{\mathrm{RS},m}+N^{-1}\varsigma_{\mathrm{RS},m}\right)+\alpha_t^{-2}P_{\mathrm{R}}^{-1}\sigma_m^2$, $\upsilon_{1_i} = \varrho_i\varsigma_{\mathrm{SR},i}$, $\upsilon_{2_i} = \varrho_i\left(\delta_{\mathrm{RS},\hat{i}}\psi_{\mathrm{SR},ii}+\delta_{\mathrm{RS},i}\psi_{\mathrm{SR},\hat{i}i}\right)$, $\upsilon_{3_i} = \left(\alpha_r^{-1}-1\right)\delta_{\mathrm{SR},i}\left[N^{-1}P_{\mathrm{R}}\sigma_{\mathrm{RR}}^2+\sigma_{\mathrm{R}}^2+\varrho_i P_{\mathrm{S}}\delta_{\mathrm{SR},i}+P_{\mathrm{S}}\sum_{j=1}^{2M}\varrho_j\beta_{\mathrm{SR},j}\right]$, and for $X\in\{\mathrm{SR},\mathrm{RS}\}$, $\psi_{X,ij}\triangleq\mathbb{E}\left\{\left|\hat{\boldsymbol{h}}_{X,i}^{\mathrm{H}}\hat{\boldsymbol{h}}_{X,j}\right|^2\right\}$, which is given by

$$\begin{aligned}\psi_{X,ij} = {} & \frac{\beta_{X,i}\beta_{X,j}}{(1+K_{X,i})(1+K_{X,j})}\Big[K_{X,i}K_{X,j}\varphi_{X,ij}^2 \\ & + N\left(K_{X,j}\Psi_{X,i}+K_{X,i}\Psi_{X,j}+\Psi_{X,i}\Psi_{X,j}\right)\Big],\end{aligned} \tag{20}$$

with

$$\varphi_{X,ij} = \frac{\sin\left[\frac{N\pi}{2}\left(\sin\left(\theta_i\right)-\sin\left(\theta_j\right)\right)\right]}{\sin\left[\frac{\pi}{2}\left(\sin\left(\theta_i\right)-\sin\left(\theta_j\right)\right)\right]}, i\neq j, \tag{21}$$

when $i=j$, there is

$$\psi_{X,ii} = \frac{N\beta_{X,i}^2\left[NK_{X,i}^2+(N+1)\left(2K_{X,i}+\Psi_{X,i}\right)\Psi_{X,i}\right]}{\left(1+K_{X,i}\right)^2}. \tag{22}$$

Proof: Refer to Appendix B.

Remark 1: Theorem 1 reveals the SE performance with imperfect CSI, imperfect SIC and low-precision ADCs/DACs, which shows that R_{SE} is a function with the transmit power of

GU and UR, the number of UR antennas, the altitude of UR, the value of Rician-K factor, the channel estimation error, the SIC level ϖ as well as the ADC/DAC resolution.

Based on Theorem 1, we can obtain the system SE for some special cases, such as perfect CSI, perfect SIC, full-precision ADCs/DACs, which are provided in the following propositions.

Proposition 1: When UR acquires the perfect CSI, the approximate closed-form expression of the sum SE with imperfect SIC and low-resolution ADCs/DACs can be given as

$$R_{\mathrm{SE}}^{(1)}=\frac{T-\tau}{T}\sum_{m=1}^{2M}\log_2\left(1+\frac{N^4\varrho_{\hat{m}}P_{\mathrm{S}}\beta_{\mathrm{RS},m}^2\beta_{\mathrm{SR},\hat{m}}^2}{\Delta_1^{(1)}+\Delta_2^{(1)}+\Delta_4^{(1)}+\Delta_5^{(1)}}\right), \quad (23)$$

where

$$\Delta_1^{(1)}=\varpi\sum_{i=1,i\neq m}^{\hat{m}-1}\sum_{j=1}^{2M}\varrho_i P_{\mathrm{S}}\psi_{\mathrm{RS},mj}^{(1)}\psi_{\mathrm{SR},\hat{j}i}^{(1)}-N^4\varrho_{\hat{m}}P_{\mathrm{S}}\times\beta_{\mathrm{RS},m}^2\beta_{\mathrm{SR},\hat{m}}^2+\sum_{i=\hat{m},i\neq m}^{2M}\sum_{j=1}^{2M}\varrho_i P_{\mathrm{S}}\psi_{\mathrm{RS},mj}^{(1)}\psi_{\mathrm{SR},\hat{j}i}^{(1)},$$

$$\Delta_2^{(1)}=N\left(P_{\mathrm{R}}\sigma_{\mathrm{RR}}^2+\sigma_{\mathrm{R}}^2\right)\left(\beta_{\mathrm{SR},\hat{m}}\psi_{\mathrm{RS},mm}^{(1)}+\beta_{\mathrm{SR},m}\psi_{\mathrm{RS},m\hat{m}}^{(1)}\right),$$

$$\Delta_4^{(1)}=\left[\left(\alpha_t^{-1}-1\right)\beta_{\mathrm{RS},m}+\alpha_t^{-2}P_{\mathrm{R}}^{-1}\sigma_m^2\right]\left[N^2\left(P_{\mathrm{R}}\sigma_{\mathrm{RR}}^2+\sigma_{\mathrm{R}}^2\right)\times\sum_{i=1}^{2M}\beta_{\mathrm{RS},i}\beta_{\mathrm{SR},\hat{i}}+N^3\sum_{i=1}^{2M}\varrho_{\hat{i}}P_{\mathrm{S}}\beta_{\mathrm{RS},i}\beta_{\mathrm{SR},\hat{i}}^2\right],$$

$$\Delta_5^{(1)}=\left(\alpha_r^{-1}-1\right)\left\{N^2\left[\left(\alpha_t^{-1}-1\right)\beta_{\mathrm{RS},m}+\alpha_t^{-2}P_{\mathrm{R}}^{-1}\sigma_m^2\right]\times\sum_{i=1}^{2M}\beta_{\mathrm{SR},i}\beta_{\mathrm{RS},i}z_i^{(1)}+N\sum_{i=1}^{2M}\beta_{\mathrm{SR},\hat{i}}\psi_{\mathrm{RS},im}^{(1)}z_i^{(1)}\right\},$$

where $z_i^{(1)}=N^{-1}P_{\mathrm{R}}\sigma_{\mathrm{RR}}^2+\sigma_{\mathrm{R}}^2+\varrho_i P_{\mathrm{S}}\beta_{\mathrm{SR},i}+\sum_{j=1}^{2M}\varrho_j P_{\mathrm{S}}\beta_{\mathrm{SR},j}$, and $\psi_{X,ij}^{(1)}$ is given by

$$\psi_{X,ij}^{(1)}=\begin{cases}\frac{\beta_{X,i}\beta_{X,j}\left[K_{X,i}K_{X,j}\varphi_{X,ij}^2+N(K_{X,i}+K_{X,j})+N\right]}{(1+K_{X,i})(1+K_{X,j})}, & i\neq j\\ N^2\beta_{X,i}^2+\frac{N\beta_{X,i}^2(2K_{X,i}+1)}{(1+K_{X,i})^2}, & i=j\end{cases} \quad (24)$$

Proposition 2: When UR performs the perfect SIC, the approximate closed-form expression of the sum SE with imperfect CSI and low-resolution ADCs/DACs can be given as

$$R_{\mathrm{SE}}^{(2)}=\frac{T-\tau}{T}\sum_{m=1}^{2M}\log_2\left(1+\frac{N^4\varrho_{\hat{m}}P_{\mathrm{S}}\delta_{\mathrm{RS},m}^2\delta_{\mathrm{SR},\hat{m}}^2}{\Delta_{\mathrm{pSIC}}^{(2)}+\Delta_4+\Delta_5}\right), \quad (25)$$

where $\Delta_{\mathrm{pSIC}}^{(2)}=\sum_{i=\hat{m},i\neq m}^{2M}\sum_{j=1}^{2M}\varrho_i P_{\mathrm{S}}\psi_{\mathrm{RS},mj}\psi_{\mathrm{SR},\hat{j}i}-N^4\varrho_{\hat{m}}P_{\mathrm{S}}\delta_{\mathrm{RS},m}^2\delta_{\mathrm{SR},\hat{m}}^2+\left(\varrho_m P_{\mathrm{S}}\varsigma_{\mathrm{SR},m}+\sum_{i=\hat{m},i\neq m}^{2M}\varrho_i P_{\mathrm{S}}\varsigma_{\mathrm{SR},i}+P_{\mathrm{R}}\sigma_{\mathrm{RR}}^2+\sigma_{\mathrm{R}}^2\right)\left(Nz_m^{(2.1)}+N^2\varsigma_{\mathrm{RS},m}\sum_{i=1}^{2M}\delta_{\mathrm{RS},i}\delta_{\mathrm{SR},\hat{i}}\right)+N\varsigma_{\mathrm{RS},m}\left(\varrho_m P_{\mathrm{S}}z_m^{(2.2)}+\sum_{i=\hat{m},i\neq m}^{2M}\varrho_i P_{\mathrm{S}}z_i^{(2.2)}\right)$, where $z_i^{(2.1)}=\delta_{\mathrm{SR},\hat{i}}\psi_{\mathrm{RS},ii}+\delta_{\mathrm{SR},i}\psi_{\mathrm{RS},i\hat{i}}$, and $z_i^{(2.2)}=\delta_{\mathrm{RS},\hat{i}}\psi_{\mathrm{SR},ii}+\delta_{\mathrm{RS},i}\psi_{\mathrm{SR},\hat{i}i}$.

Proposition 3: When UR is equipped with full-precision ADCs/DACs, while imperfect CSI and imperfect SIC are also considered, the approximate closed-form expression of the sum SE can be given as

$$R_{\mathrm{SE}}^{(3)}=\frac{T-\tau}{T}\sum_{m=1}^{2M}\log_2\left(1+\frac{N^4\varrho_{\hat{m}}P_{\mathrm{S}}\eta_{\mathrm{RS},m}^2\eta_{\mathrm{SR},\hat{m}}^2}{\Delta_1^{(3)}+\Delta_2^{(3)}+\Delta_3^{(3)}}\right), \quad (26)$$

where

$$\Delta_1^{(3)}=\varpi\sum_{i=1,i\neq m}^{\hat{m}-1}\sum_{j=1}^{2M}\varrho_i P_{\mathrm{S}}\psi_{\mathrm{RS},mj}^{(3)}\psi_{\mathrm{SR},\hat{j}i}^{(3)}-N^4\varrho_{\hat{m}}P_{\mathrm{S}}\times\eta_{\mathrm{RS},m}^2\eta_{\mathrm{SR},\hat{m}}^2+\sum_{i=\hat{m},i\neq m}^{2M}\sum_{j=1}^{2M}\varrho_i P_{\mathrm{S}}\psi_{\mathrm{RS},mj}^{(3)}\psi_{\mathrm{SR},\hat{j}i}^{(3)},$$

$$\Delta_2^{(3)}=\left[N\left(\eta_{\mathrm{SR},\hat{m}}\psi_{\mathrm{RS},mm}^{(3)}+\eta_{\mathrm{SR},m}\psi_{\mathrm{RS},m\hat{m}}^{(3)}\right)+N^2\xi_{\mathrm{RS},m}\times\sum_{i=1}^{2M}\eta_{\mathrm{RS},i}\eta_{\mathrm{SR},\hat{i}}\right]\left[P_{\mathrm{R}}\sigma_{\mathrm{RR}}^2+\sigma_{\mathrm{R}}^2+P_{\mathrm{S}}\left(\varrho_m\xi_{\mathrm{SR},m}+\varpi\sum_{i=1,i\neq m}^{\hat{m}-1}\varrho_i\xi_{\mathrm{SR},i}+\sum_{i=\hat{m},i\neq m}^{2M}\varrho_i\xi_{\mathrm{SR},i}\right)\right],$$

$$\Delta_3^{(3)}=\varpi N\xi_{\mathrm{RS},m}P_{\mathrm{S}}\sum_{i=1,i\neq m}^{\hat{m}-1}z_i^{(3)}+N\xi_{\mathrm{RS},m}P_{\mathrm{S}}z_m^{(3)}+N\xi_{\mathrm{RS},m}P_{\mathrm{S}}\sum_{i=\hat{m},i\neq m}^{2M}z_i^{(3)},$$

where $z_i^{(3)}=\varrho_i\left(\eta_{\mathrm{RS},\hat{i}}\psi_{\mathrm{SR},ii}^{(3)}+\eta_{\mathrm{RS},i}\psi_{\mathrm{SR},\hat{i}i}^{(3)}\right)$. $\eta_{X,i}=\frac{K_{X,i}\beta_{X,i}+(1+K_{X,i})\alpha_{\mathbf{\Phi},i}P_{\mathbf{\Phi}}\beta_{X,i}^2}{(1+K_{X,i})(1+\alpha_{\mathbf{\Phi},i}P_{\mathbf{\Phi}}\beta_{X,i})}$, $X\in\{\mathrm{SR},\mathrm{RS}\}$, $\xi_{X,i}=\frac{\beta_{X,i}}{(1+K_{X,i})(1+\alpha_{\mathbf{\Phi},i}P_{\mathbf{\Phi}}\beta_{X,i})}$, and $\psi_{X,ij}^{(3)}$ is given by (27), shown on the top of next page, where $\Gamma_{X,i}\triangleq\alpha_{\mathbf{\Phi},i}P_{\mathbf{\Phi}}\beta_{X,i}/(1+\alpha_{\mathbf{\Phi},i}P_{\mathbf{\Phi}}\beta_{X,i})$.

B. Asymptotic Analysis

To further study the effect of system parameters on SE performance, we also derive some asymptotic results according to Theorem 1, which are shown in the following corollaries.

Corollary 1: When the transmit power of GUs and UR tend to infinity (i.e., $P_{\mathrm{S}}=P_{\mathrm{R}}\to\infty$, denoted as $P\to\infty$), the asymptotic SE under imperfect CSI, imperfect SIC and low-resolution ADCs/DACs is given as

$$R_{\mathrm{SE}}^{P\to\infty}=\frac{T-\tau}{T}\sum_{m=1}^{2M}\log_2\left(1+\frac{N^4\varrho_{\hat{m}}\delta_{\mathrm{RS},m}^2\delta_{\mathrm{SR},\hat{m}}^2}{\Pi_1+\Pi_2+\Pi_3+\Pi_4+\Pi_5}\right), \quad (28)$$

where

$$\Pi_1=\varpi\sum_{i=1,i\neq m}^{\hat{m}-1}\sum_{j=1}^{2M}\varrho_i\psi_{\mathrm{RS},mj}\psi_{\mathrm{SR},\hat{j}i}-N^4\varrho_{\hat{m}}\delta_{\mathrm{RS},m}^2\times\delta_{\mathrm{SR},\hat{m}}^2+\sum_{i=\hat{m},i\neq m}^{2M}\sum_{j=1}^{2M}\varrho_i\psi_{\mathrm{RS},mj}\psi_{\mathrm{SR},\hat{j}i},$$

$$\Pi_2=\left(\varpi\sum_{i=1,i\neq m}^{\hat{m}-1}\upsilon_{1_i}+\upsilon_{1_m}+\sum_{i=\hat{m},i\neq m}^{2M}\upsilon_{1_i}+\sigma_{\mathrm{RR}}^2\right)\times\left[N(\delta_{\mathrm{SR},\hat{m}}\psi_{\mathrm{RS},mm}+\delta_{\mathrm{SR},m}\psi_{\mathrm{RS},m\hat{m}})+\Omega\varsigma_{\mathrm{RS},m}\right],$$

$$\Pi_3=N\varsigma_{\mathrm{RS},m}\left(\varpi\sum_{i=1,i\neq m}^{\hat{m}-1}\upsilon_{2_i}+\upsilon_{2_m}+\sum_{i=\hat{m},i\neq m}^{2M}\upsilon_{2_i}\right),$$

$$\Pi_4=\tilde{J}_m\left[\Omega\left(\sum_{i=1}^{2M}\upsilon_{1_i}+\sigma_{\mathrm{RR}}^2\right)+N^2\sum_{i=1}^{2M}\delta_{\mathrm{RS},i}\tilde{\upsilon}_{3_i}+N^3\times\sum_{i=1}^{2M}\varrho_{\hat{i}}\delta_{\mathrm{RS},i}\delta_{\mathrm{SR},\hat{i}}^2\right],$$

$$\Pi_5=N\sum_{i=1}^{2M}\left(\psi_{\mathrm{RS},im}\tilde{\upsilon}_{3_{\hat{i}}}+N\varsigma_{\mathrm{RS},m}\delta_{\mathrm{RS},i}\tilde{\upsilon}_{3_i}\right),$$

where $\psi_{\mathrm{SR},ij}$, $\psi_{\mathrm{RS},ij}$, υ_{1_i}, υ_{2_i}, Ω are the same as those given in Theorem 1, $\tilde{J}_m=\left(\alpha_t^{-1}-1\right)\left(\delta_{\mathrm{RS},m}+N^{-1}\varsigma_{\mathrm{RS},m}\right)$, $\tilde{\upsilon}_{3_i}=\left(\alpha_r^{-1}-1\right)\delta_{\mathrm{SR},i}\left(\varrho_i\delta_{\mathrm{SR},i}+\sum_{j=1}^{2M}\varrho_j\beta_{\mathrm{SR},j}+N^{-1}\sigma_{\mathrm{RR}}^2\right)$.

Remark 2: From Corollary 1, the system SE tends to be constant as the transmit power of GUs and UR increases. This constant value is limited by the number of ADC/DAC quantization bits, channel estimation errors, inter-pair interference between different GU pairs, and RSI at the FD UR.

$$\psi_{X,ij}^{(3)}=\begin{cases}\frac{\beta_{X,i}\beta_{X,j}\left[K_{X,i}K_{X,j}\varphi_{X,ij}^{2}+N(K_{X,j}\Gamma_{X,i}+K_{X,i}\Gamma_{X,j}+\Gamma_{X,i}\Gamma_{X,j})\right]}{(1+K_{X,i})(1+K_{X,j})}, & i\neq j\\ \frac{N\beta_{X,i}^{2}\left[NK_{X,i}^{2}+(N+1)(2K_{X,i}+\Gamma_{X,i})\Gamma_{X,i}\right]}{(1+K_{X,i})^{2}}, & i=j\end{cases} \tag{27}$$

This also shows that the effect of quantization noise on system SE cannot be completely eliminated by simply increasing the transmit power of GU and UR. Finally, substituting $P\to\infty$ into (23), (25) and (26), we can obtain the results under perfect CSI, perfect SIC, full-precision ADCs/DACs, respectively.

Corollary 2: When UR is equipped with massive antennas, the asymptotic SE under imperfect CSI, imperfect SIC and low-resolution ADCs/DACs is expressed as

$$R_{\mathrm{SE}}^{N\to\infty}=\frac{T-\tau}{T}\sum_{m=1}^{2M}\log_2\left(1+\frac{\varrho_{\hat{m}}P_{\mathrm{S}}\delta_{\mathrm{RS},m}^{2}\delta_{\mathrm{SR},\hat{m}}^{2}}{\Sigma_1+\Sigma_2+\Sigma_3+\Sigma_4+\Sigma_5}\right), \tag{29}$$

where

$$\begin{aligned}\Sigma_1&=\left(N^{-1}\delta_{\mathrm{RS},m}^{2}\delta_{\mathrm{SR},\hat{m}}+N^{-2}\varsigma_{\mathrm{RS},m}\sum\nolimits_{i=1}^{2M}\delta_{\mathrm{RS},i}\delta_{\mathrm{SR},\hat{i}}\right)\Big[P_{\mathrm{S}}\\&\quad\times\left(\varpi\sum\nolimits_{i=1,i\neq m}^{\hat{m}-1}\upsilon_{1_i}+\upsilon_{1_m}+\sum\nolimits_{i=\hat{m},i\neq m}^{2M}\upsilon_{1_i}\right)+\Theta\Big],\\\Sigma_2&=N^{-1}\varsigma_{\mathrm{RS},m}P_{\mathrm{S}}\Big(\varpi\sum\nolimits_{i=1,i\neq m}^{\hat{m}-1}\varrho_i\delta_{\mathrm{SR},i}^{2}\delta_{\mathrm{RS},\hat{i}}+\varrho_m\delta_{\mathrm{SR},m}^{2}\\&\quad\times\delta_{\mathrm{RS},\hat{m}}+\sum\nolimits_{i=\hat{m},i\neq m}^{2M}\varrho_i\delta_{\mathrm{SR},i}^{2}\delta_{\mathrm{RS},\hat{i}}\Big),\\\Sigma_3&=\Big[P_{\mathrm{S}}\sum\nolimits_{i=1}^{2M}\varrho_{\hat{i}}\delta_{\mathrm{RS},i}\delta_{\mathrm{SR},\hat{i}}^{2}+N^{-1}\sum\nolimits_{i=1}^{2M}\delta_{\mathrm{RS},i}\delta_{\mathrm{SR},\hat{i}}\Big(P_{\mathrm{S}}\\&\quad\times\sum\nolimits_{i=1}^{2M}\upsilon_{1_i}+\Theta\Big)\Big]\left[N^{-2}\left(\alpha_t^{-1}-1\right)\varsigma_{\mathrm{RS},m}+N^{-1}\bar{J}_m\right],\\\Sigma_4&=\left(\alpha_r^{-1}-1\right)\Big[\left(\alpha_t^{-1}-1\right)\left(\delta_{\mathrm{RS},m}+N^{-1}\varsigma_{\mathrm{RS},m}\right)+\varsigma_{\mathrm{RS},m}\\&\quad+\alpha_t^{-2}P_{\mathrm{R}}^{-1}\sigma_m^{2}\Big]\sum\nolimits_{i=1}^{2M}\delta_{\mathrm{RS},i}\left(N^{-3}P_{\mathrm{R}}\sigma_{\mathrm{RR}}^{2}\delta_{\mathrm{SR},i}+N^{-2}\bar{\upsilon}_{3_i}\right),\\\Sigma_5&=\Big[P_{\mathrm{S}}\Big(\varrho_{\hat{m}}\delta_{\mathrm{SR},\hat{m}}+\sum\nolimits_{j=1}^{2M}\varrho_j\beta_{\mathrm{SR},j}\Big)+\sigma_{\mathrm{R}}^{2}+N^{-1}P_{\mathrm{R}}\sigma_{\mathrm{RR}}^{2}\Big]\\&\quad\times N^{-1}\left(\alpha_r^{-1}-1\right)\delta_{\mathrm{RS},m}^{2}\delta_{\mathrm{SR},\hat{m}},\end{aligned}$$

where $\bar{J}_m=\left(\alpha_t^{-1}-1\right)\delta_{\mathrm{RS},m}+\alpha_t^{-2}P_{\mathrm{R}}^{-1}\sigma_m^{2}$, $\bar{\upsilon}_{3_i}=\delta_{\mathrm{SR},i}\big[\sigma_{\mathrm{R}}^{2}+P_{\mathrm{S}}\big(\varrho_i\delta_{\mathrm{SR},i}+\sum_{j=1}^{2M}\varrho_j\beta_{\mathrm{SR},j}\big)\big]$.

Remark 3: Corollary 2 shows that the sum SE grows when N tends to infinity. This means that the SE loss due to low quantization can be compensated by employing more antennas at UR. Moreover, substituting $N\to\infty$ into Propositions 1-3, the corresponding asymptotic results can be obtained.

Corollary 3: When the number of quantization bits tends to infinite, the asymptotic SE under imperfect CSI and imperfect SIC is same as (26), that is, $R_{\mathrm{SE}}^{b\to\infty}=R_{\mathrm{SE}}^{(3)}$.

Remark 4: Corollary 3 derives an asymptotic expression for the system SE when $b\to\infty$. This represents that UR is equipped with full-precision ADCs/DACs, which can be used as a baseline to measure the degree of impact of quantization noise on the system performance.

C. Power Scaling Law

To analyze the possible power savings during the data transmission phase and the interaction between the transmit power of GUs and UR, we give the power scaling law for UAV-enabled massive MIMO-NOMA FD TWR system in the following corollaries.

Corollary 4: When $P_{\mathrm{S}}=E_{\mathrm{S}}/N^{\varepsilon_{\mathrm{S}}}$ and $P_{\mathrm{R}}=E_{\mathrm{R}}/N^{\varepsilon_{\mathrm{R}}}$, fixed E_{S}, E_{R}, while $0\leq\varepsilon_{\mathrm{S}},\varepsilon_{\mathrm{R}}\leq 1$, as N grows into infinity, the asymptotic SE under imperfect CSI, imperfect SIC and low-resolution ADCs/DACs can be derived as

$$\tilde{R}_{\mathrm{SE}}=\frac{T-\tau}{T}\sum_{m=1}^{2M}\log_2\left(1+\frac{\varrho_{\hat{m}}\delta_{\mathrm{RS},m}^{2}\delta_{\mathrm{SR},\hat{m}}^{2}}{\tilde{\Sigma}_1+\tilde{\Sigma}_3+\tilde{\Sigma}_4+\tilde{\Sigma}_5}\right), \tag{30}$$

where

$$\begin{aligned}\tilde{\Sigma}_1&=\left(N^{\varepsilon_{\mathrm{S}}-\varepsilon_{\mathrm{R}}-1}E_{\mathrm{R}}\sigma_{\mathrm{RR}}^{2}+N^{\varepsilon_{\mathrm{S}}-1}\sigma_{\mathrm{R}}^{2}\right)E_{\mathrm{S}}^{-1}\delta_{\mathrm{RS},m}^{2}\delta_{\mathrm{SR},\hat{m}},\\\tilde{\Sigma}_3&=\alpha_t^{-2}E_{\mathrm{R}}^{-1}\sigma_m^{2}\Big(N^{\varepsilon_{\mathrm{R}}-1}\sum\nolimits_{i=1}^{2M}\varrho_{\hat{i}}\delta_{\mathrm{RS},i}\delta_{\mathrm{SR},\hat{i}}^{2}+N^{\varepsilon_{\mathrm{S}}+\varepsilon_{\mathrm{R}}-2}\\&\quad\times E_{\mathrm{S}}^{-1}\sigma_{\mathrm{R}}^{2}\sum\nolimits_{i=1}^{2M}\delta_{\mathrm{RS},i}\delta_{\mathrm{SR},\hat{i}}\Big),\\\tilde{\Sigma}_4&=\left(\alpha_r^{-1}-1\right)\alpha_t^{-2}N^{\varepsilon_{\mathrm{S}}+\varepsilon_{\mathrm{R}}-2}E_{\mathrm{S}}^{-1}E_{\mathrm{R}}^{-1}\sigma_m^{2}\sigma_{\mathrm{R}}^{2}\sum\nolimits_{i=1}^{2M}\delta_{\mathrm{RS},i}\delta_{\mathrm{SR},i},\\\tilde{\Sigma}_5&=\left(\alpha_r^{-1}-1\right)N^{\varepsilon_{\mathrm{S}}-1}E_{\mathrm{S}}^{-1}\sigma_{\mathrm{R}}^{2}\delta_{\mathrm{RS},m}^{2}\delta_{\mathrm{SR},\hat{m}}.\end{aligned}$$

From Corollary 4, the asymptotic SE can be obtained for the following four cases:

(i) ***Case*** 1: When $\varepsilon_{\mathrm{S}}=\varepsilon_{\mathrm{R}}=1$, we have

$$\tilde{R}_{\mathrm{SE}}^{(1)}=\frac{T-\tau}{T}\sum_{m=1}^{2M}\log_2\left(1+\frac{\varrho_{\hat{m}}E_{\mathrm{S}}E_{\mathrm{R}}\delta_{\mathrm{RS},m}^{2}\delta_{\mathrm{SR},\hat{m}}^{2}}{\Sigma^{(1)}}\right), \tag{31}$$

where $\Sigma^{(1)}=E_{\mathrm{R}}\sigma_{\mathrm{R}}^{2}\delta_{\mathrm{RS},m}^{2}\delta_{\mathrm{SR},\hat{m}}+\alpha_t^{-2}\sigma_m^{2}\times\left(E_{\mathrm{S}}\sum_{i=1}^{2M}\varrho_{\hat{i}}\delta_{\mathrm{RS},i}\delta_{\mathrm{SR},\hat{i}}^{2}+\sigma_{\mathrm{R}}^{2}\sum_{i=1}^{2M}\delta_{\mathrm{RS},i}\delta_{\mathrm{SR},\hat{i}}\right)+\left(\alpha_r^{-1}-1\right)\times\left(\alpha_t^{-2}\sigma_{\mathrm{R}}^{2}\sigma_m^{2}\sum_{i=1}^{2M}\delta_{\mathrm{RS},i}\delta_{\mathrm{SR},i}+E_{\mathrm{R}}\sigma_{\mathrm{R}}^{2}\delta_{\mathrm{RS},m}^{2}\delta_{\mathrm{SR},\hat{m}}\right)$.

(ii) ***Case*** 2: When $0\leq\varepsilon_{\mathrm{S}}<1$, $\varepsilon_{\mathrm{R}}=1$, we have

$$\tilde{R}_{\mathrm{SE}}^{(2)}=\frac{T-\tau}{T}\sum_{m=1}^{2M}\log_2\left(1+\frac{\varrho_{\hat{m}}E_{\mathrm{R}}\delta_{\mathrm{RS},m}^{2}\delta_{\mathrm{SR},\hat{m}}^{2}}{\alpha_t^{-2}\sigma_m^{2}\sum\limits_{i=1}^{2M}\varrho_{\hat{i}}\delta_{\mathrm{RS},i}\delta_{\mathrm{SR},\hat{i}}^{2}}\right). \tag{32}$$

(iii) ***Case*** 3: When $\varepsilon_{\mathrm{S}}=1$, $0\leq\varepsilon_{\mathrm{R}}<1$, we have

$$\tilde{R}_{\mathrm{SE}}^{(3)}=\frac{T-\tau}{T}\sum_{m=1}^{2M}\log_2\left(1+\frac{\varrho_{\hat{m}}E_{\mathrm{S}}\delta_{\mathrm{SR},\hat{m}}}{E_{\mathrm{R}}\sigma_{\mathrm{RR}}^{2}+\alpha_r^{-1}\sigma_{\mathrm{R}}^{2}}\right). \tag{33}$$

(iv) ***Case*** 4: When $0<\varepsilon_{\mathrm{S}}<1$, $0<\varepsilon_{\mathrm{R}}<1$ or $\varepsilon_{\mathrm{S}}=\varepsilon_{\mathrm{R}}=0$, we have $\tilde{R}_{\mathrm{SE}}^{(4)}\to\infty$.

Remark 5: Corollary 4 characterizes the power scaling law of the considered system with imperfect CSI, imperfect SIC and low-resolution ADCs/DACs. As $N\to\infty$, the results in Cases 1$\sim$3 all converge to deterministic constants, while the system SE grows unboundedly in Case 4. This indicates that the SE performance is related to the scaling parameters, ε_{S} and ε_{R}: the transmit power of GU and UR can be scaled down proportionally to $1/N^{\varepsilon_{\mathrm{S}}}$ and $1/N^{\varepsilon_{\mathrm{R}}}$ ($\varepsilon_{\mathrm{S}}=1$, $0\leq\varepsilon_{\mathrm{R}}\leq 1$ or $\varepsilon_{\mathrm{R}}=1$, $0\leq\varepsilon_{\mathrm{S}}\leq 1$), respectively, to maintain the expected SE.

TABLE II
SIMULATION PARAMETERS

Parameters	Values
Number of the GU pairs	$M = 3$
Altitude of the UAV	$H = 100$ m
Position of the UAV	$\boldsymbol{u} = (0, 0, H)$
Coordinate range of the GU	$\|\|\boldsymbol{q}_i\|\| \leq 150$
Reference channel power gain	$\beta_0 = -30$ dB
Environmental parameters	$c_1 = 9.61, c_2 = 0.16$
Attenuation factors	$\eta_{\mathrm{L}} = 1, \eta_{\mathrm{NL}} = 0.7$
Path loss exponent	$k = 3$
Length of coherence interval	$T = 200$
Length of training interval	$\tau = 2M$
Rician factor	$K_{X,i} \triangleq K = 10$ dB
Interference and noise	$\sigma_{\mathrm{RR}}^2 = \sigma_{\mathrm{R}}^2 = \sigma_i^2 = 0$ dB
Mixer power	$P_{\mathrm{mix}} = 30.3$ mW
Active filter power at the transmitter/receiver side	$P_{\mathrm{filt}} = P_{\mathrm{filr}} = 2.5$ mW
Frequency synthesizer power	$P_{\mathrm{syn}} = 50$ mW
Low-noise amplifier power	$P_{\mathrm{LNA}} = 20$ mW
Intermediate frequency amplifier power	$P_{\mathrm{IFA}} = 3$ mW
Automatic gain control power	$P_{\mathrm{AGC}} = 2$ mW
Power supply of converter	$V_{\mathrm{dd}} = 3$ V
Minimum channel length for CMOS	$L_{\mathrm{min}} = 0.5$ μA
Corner frequency	$f_{\mathrm{cor}} = 1$ MHz
Unit current source	$I_0 = 10$ μA
Parasitic capacitance	$C_{\mathrm{p}} = 1$ pF

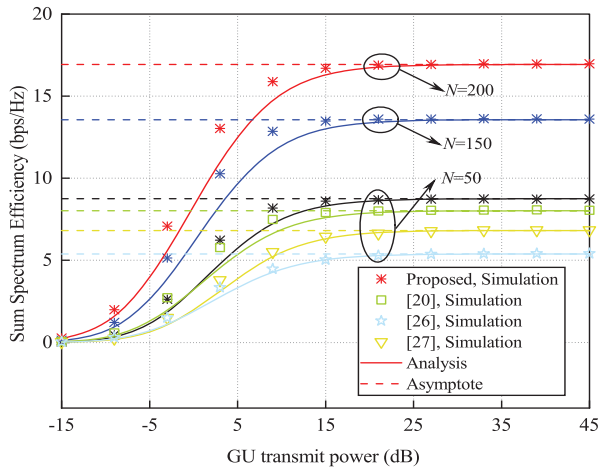

Fig. 2. Sum SE versus P_{S} varying N for $P_{\Phi} = P_{\mathrm{S}}, P_{\mathrm{R}} = P_{\mathrm{S}}, b = 1$.

IV. NUMERICAL RESULTS

In this section, some numerical results are provided to validate the correctness of the proposed system. Unless mentioned otherwise, the simulation parameters are set as in Table II. In addition, the fixed power allocation is employed for M pairs' NOMA GUs, and the power allocation factors are satisfy $\varrho_i = \frac{2M-i+1}{\chi}$, where $\chi = \sum_{i=1}^{2M}(2M - i + 1)$.

A. Spectrum Efficiency

a. NOMA v.s. OMA, FD v.s. HD

Fig. 2 shows the simulated, analytical and asymptotic sum SE versus total GU transmit power P_{S} for FD TWR massive MIMO-NOMA systems with 1-bit ADCs/DACs, which is based on the imperfect CSI and imperfect SIC cases. To facilitate comparison, the results of the OMA-MIMO-FD [21], OMA-MIMO-HD-TWR [27] and NOMA-MIMO-HD-TWR [28] schemes are also provided under the same network setting. Note that the transmit power of each GU (defined as $p_i, i = 1, 2, \ldots 2M$) is set to be the same in the OMA scheme, i.e., $p_i = P_{\mathrm{S}}/2M$. For the proposed scheme, the three curves for different number of UR antennas are obtained according to (18), (19) and (29), respectively. As shown in Fig. 2, in the presence of quantization noise, the proposed scheme gains superior SE performance compared with the other three transmission schemes. This proves the performance advantages of the proposed scheme. In addition, the sum SE first grows rapidly and then slowly converges to a fixed value as P_{S} increases, which is consistent with Corollary 1. The saturation is caused by the interference among different GU pairs, the RSI on the FD UAV, the channel estimation errors, and the ADC/DAC distortion. Meanwhile, the effects of these interference and distortion components do not attenuate when the transmit power increases.

b. Perfect SIC v.s. Imperfect SIC

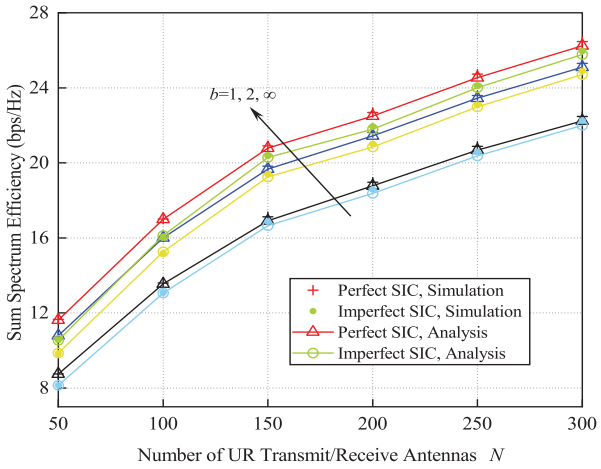

Fig. 3. Sum SE versus N varying b under both perfect and imperfect SIC for $P_{\Phi} = P_{\mathrm{S}} = P_{\mathrm{R}} = 30$ dB.

Fig. 3 presents the effect of the number of UR antennas N on the sum SE for different ADC/DAC resolution bits b with both perfect and imperfect SIC. For imperfect SIC, we set $\varpi = 0.9$. Compared with perfect SIC, there is a certain SE loss caused by SIC error. An insightful observation is that quantization error deteriorates the SE performance more than SIC error when N is large. This is because when the UR is configured with large-scale antennas in the presence of low-resolution ADCs/DACs, the quantization noise has a dominant limiting effect compared with the inter-user interference caused by imperfect SIC. One can also observe that the SE of all cases increases significantly from $b = 1$ to 2. However, the gaps between $b = 2$ and $b \to \infty$ becomes narrow. This indicates that the SE loss caused by quantization noise decreases as b increases. Furthermore, the limited SE loss due to the quantization noise can be compensated by increasing N. For example, in the perfect SIC case, when using infinite resolution ADCs/DACs, the UR requires about

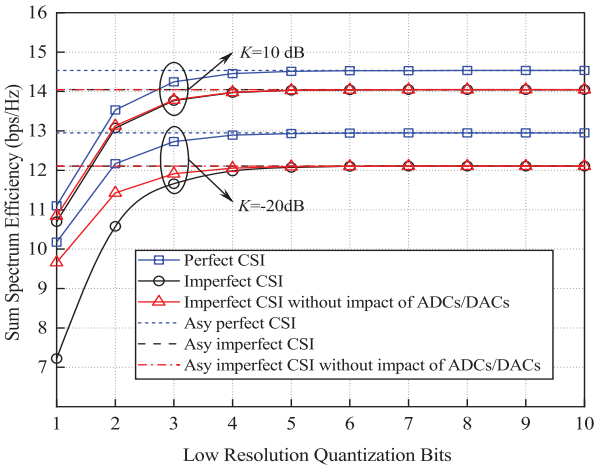

Fig. 4. Sum SE versus b varying K for $N = 64, P_\Phi = P_S = P_R = 30$ dB.

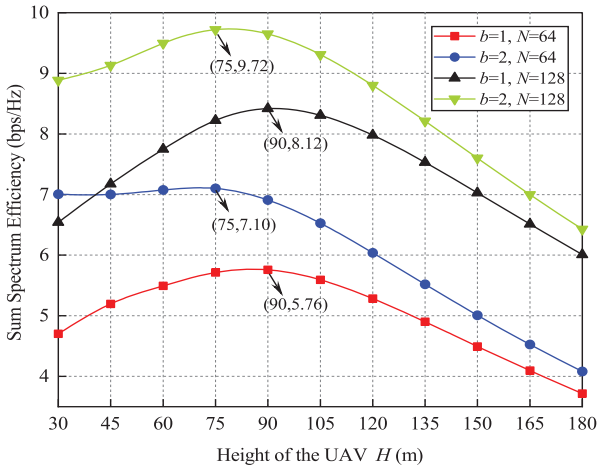

Fig. 5. Sum SE versus H varying b and N for $M = 2, P_\Phi = P_S = P_R = 30$ dB.

150 receive/transmit antennas to attain a sum SE of 21 bps/Hz, while for 2-bit ADC/DAC resolution, it needs about 200 receive/transmit antennas to reach the same sum SE.

c. Different CSI Cases

Fig. 4 compares the sum SE versus various ADC/DAC resolution levels for three CSI cases: (i) perfect CSI, (ii) imperfect CSI, and (iii) estimated CSI without considering the impact of quantization noise. Noted that the "Asy" curves mean the asymptotic results when $b \to \infty$, and the curves with $K = -20$ dB represent the results under Rayleigh channel [17], [18]. As expected, the Rayleigh fading has smaller SE value, because the larger the value of K, the stronger the LoS component. We observe that all the curves converge to fixed values as b increases, and the performance comparable to full-precision ADCs/DACs can be achieved when b is almost 5. Meanwhile, the SE performance is much worse when $b = 1$ or 2 compared to the coarse quantization bits, because low quantization bits result in a significant reduction in the accuracy of the channel estimation.

d. Impact of ADC/DAC Distortion (four cases of power scaling law)

To further explore the effects of ADC/DAC distortions under different parameter conditions, we provide Figs. 5-7.

Fig. 5 shows the sum SE versus the height of the UAV for different quantization bits. It can observe that the sum SE first increases and then decreases with the increase of UAV height H, which implies that there exists an optimal operating altitude to enhance SE performance. The reason is that as H grows, the performance improvement from LoS link transmission is more dominant than the path-loss due to increased distance. However, when H continues to increase beyond the optimal operating altitude, the SE performance is limited mainly by the increase of distance. Another observation is that the optimal operating altitude of the UAV varies at different quantization levels, as shown by the coordinate points labeled in Fig. 5. Moreover, the sum SE deteriorates as the ADC/DAC resolution reduces. This can be improved by properly adjusting the height

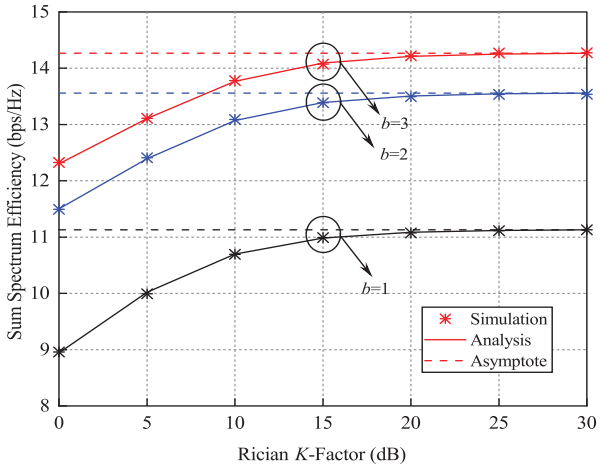

Fig. 6. Sum SE versus K varying b for $M = 3, N = 64, P_\Phi = P_S = P_R = 30$ dB.

of the UAV. For instance, the sum SE of 2-bit system is about 5.52 bps/Hz at $H = 135$ m, $N = 64$, and the same SE performance can be achieved through reducing the height by about 30 m when $b = 1$.

Fig. 6 illustrates that the sum SE at any ADC/DAC resolution can be significantly improved when the value of Rician K-factor increases. The "Asymptote" is obtained as $K \to \infty$. This suggests that the sum SE approaches a constant when the channel has only LoS components. Also, the gap between $b = 1$ and $b = 2$ is obviously larger than that between $b = 2$ and $b = 3$, and these gaps tend to a fixed value as K increases. Moreover, the 3-bit system can achieve a SE of about 13.11 bps/Hz at $K = 5$ dB, and when $b = 2$, the system can realize the same SE performance by increasing the Rician factor to 10 dB. This demonstrates that the SE loss due to low-resolution ADCs/DACs can be improved by increasing K.

Fig. 7 shows the power scaling law for four cases in Corollary 4, which revealed that the use of massive antennas at UR can result in significant power savings. Particularly, for case 1,

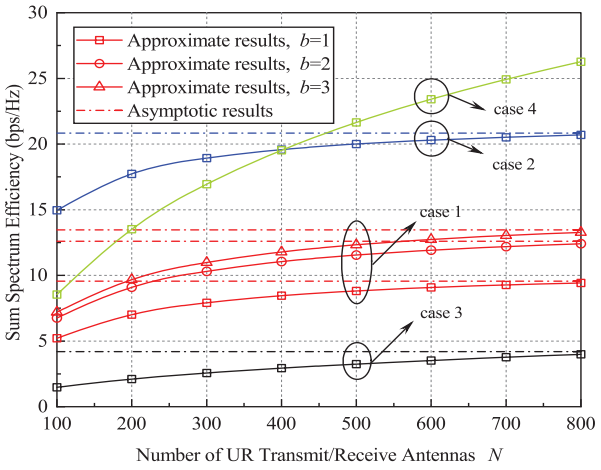

Fig. 7. Sum SE versus N varying b for $M = 4$, $P_\Phi = 20$ dB, $P_{\rm S} = E_{\rm S}/N^{\varepsilon_{\rm S}}$ with $E_{\rm S} = 20$ dB, and $P_{\rm R} = E_{\rm R}/N^{\varepsilon_{\rm R}}$ with $E_{\rm R} = 25$ dB.

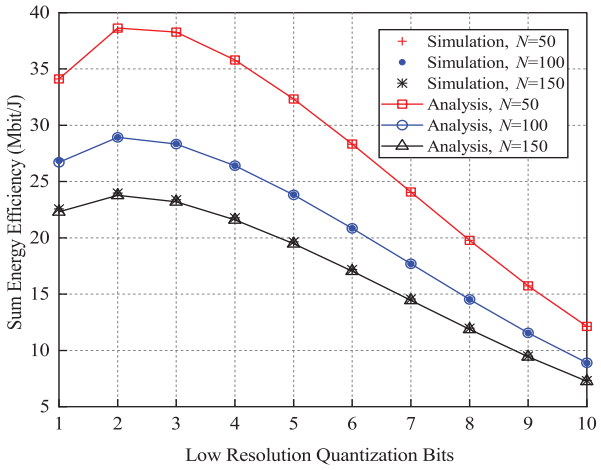

Fig. 8. EE versus ADC/DAC resolution quantization bits varying N for $P_\Phi = P_{\rm S} = P_{\rm R} = 30$ dB.

i.e., $\varepsilon_{\rm S} = \varepsilon_{\rm R} = 1$, the results are given for different ADC/DAC resolution levels. We can observe that the curves for $b = 1$ and $b = 2$ (or 3) still tend to different values. This indicates that the effect of low-resolution ADCs/DACs cannot be completely eliminated, but the SE loss can be effectively compensated by increasing N. The required number of UR antennas is related to the ADC/DAC resolution levels. For instance, compared to $b = 3$, the 1-bit system needs approximately fourfold antennas to achieve a sum SE of 9.55 bps/Hz, while the 2-bit system requires only about 40 additional antennas.

B. Energy Efficiency

The EE of the wireless communication systems can be defined as

$$\eta_{\rm EE} = \frac{R_{\rm SE} B}{P_{\rm tot}}, \tag{34}$$

where $R_{\rm SE}$ represents the sum SE, B refers to the transmission bandwidth assumed to be 20 MHz [22], and $P_{\rm tot}$ is the total power consumption of the UR RF chains for signal processing. Combining [29] (Eq. (72)) and [30] (Eq. (9)), like [22] (Eq. (32)), $P_{\rm tot}$ can be expressed as

$$\begin{aligned} P_{\rm tot} =& N\left(P_{\rm mix} + P_{\rm filt}\right) + 2P_{\rm syn} \\ &+ N\left(P_{\rm LNA} + P_{\rm mix} + P_{\rm IFA} + P_{\rm filr}\right) \\ &+ N\left[\left(c_{\rm A} + c_{\rm D}\right) P_{\rm AGC} + P_{\rm ADC} + P_{\rm DAC}\right], \end{aligned} \tag{35}$$

where the expressions for $P_{\rm ADC}$, $P_{\rm DAC}$ are referred to [31]:

$$P_{\rm ADC} = \frac{3V_{\rm dd}^2 L_{\min}\left(2B + f_{\rm cor}\right)}{10^{-0.1525b+4.838}}, \tag{36}$$

$$P_{\rm DAC} = \frac{1}{2} V_{\rm dd} I_0 \left(2^b - 1\right) + bC_{\rm p}\left(2B + f_{\rm cor}\right) V_{\rm dd}^2, \tag{37}$$

where the definitions and simulation values of all parameters are shown in Table II. In addition, $c_{\rm A}/c_{\rm D}$ denotes the flag related to quantization bits of low-resolution ADCs/DACs, which can be given as $c_{\rm A} = c_{\rm D} \triangleq c = \begin{cases} 0, & b = 1 \\ 1, & b > 1 \end{cases}$.

In Fig. 8, we plot the curves of EE with resolution level, and investigate the effect of different number of UR transmit

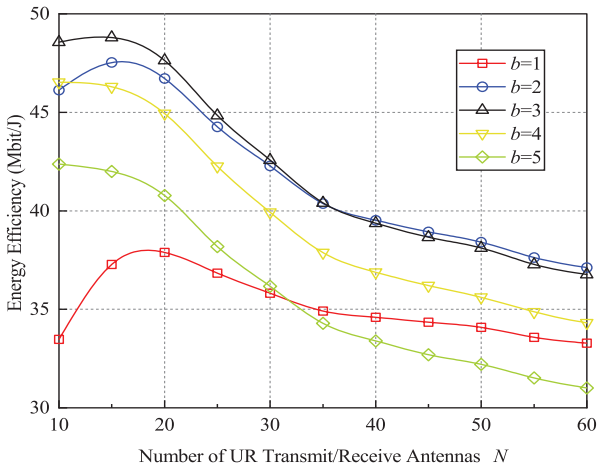

Fig. 9. EE versus N varying b for $P_\Phi = P_{\rm S} = P_{\rm R} = 30$ dB.

(receive) antennas on EE. It can be seen that the EE curves rise initially and then decrease as the resolution increases. In addition, more UR antennas result in lower EE. This is due to the power consumption of the UR RF chains used for signal processing increases linearly with N, while the sum SE has a logarithmic scale for N. Fig. 9 further explores the system parameters for achieving the best EE. The fact can be found that the 1, 2, 3-bit system can achieve its optimal EE when the UR is configured with about 40, 30 and 30 antennas.

Fig. 10 demonstrates the trade-off between EE and SE in the presence of low-resolution ADCs/DACs for different number of the UR transmit (receive) antennas N, Rician K-factor, and quantization bits b. For each case, the excellent sum SE value is displayed at the rightmost point, while the best EE value is given at the topmost point. Thus, the best EE/SE trade-off is achieved roughly at the top rightmost point, and a slight sacrifice of SE is required to obtain a higher EE value. Specifically, both the sum SE and EE increase when $b = 1$ to 2 (or 3). However, with a further increase of the

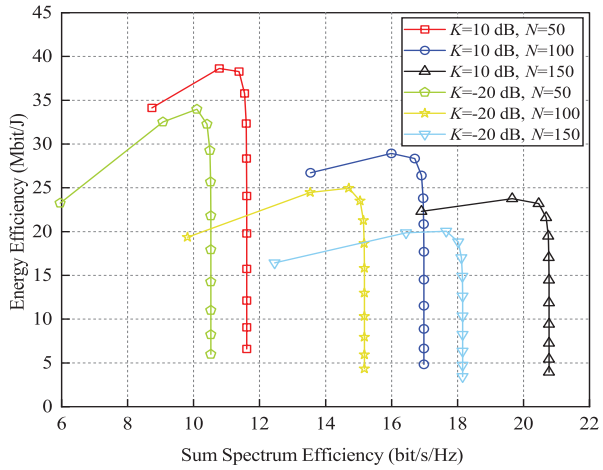

Fig. 10. Trade-off between EE and SE with low-resolution ADCs/DACs for $P_\Phi = P_S = P_R = 30$ dB.

ADC/DAC resolution, the EE decreases rapidly, while the sum SE gradually remains at a constant value. The reason is that the sum SE is a sub-linear increasing function of b, while the power consumption of the ADCs/DACs grows exponentially with increasing b. Furthermore, the optimal quantization bits influenced by both the number of UR antennas and the Rician K-factor. It is clear from Fig. 10 that the sum SE improves and the EE deteriorates as N increases. This is consistent with the findings in Figs. 4 and 8, where increasing the UR antenna number results in a higher SE gain than the EE gain. As expected, the envelope of the EE/SE region grows as K increases, which is due to larger K values can achieve higher SE as shown in Fig. 6. That is, the system with low-resolution ADC/DAC architecture has a larger operating region when operating in Rician fading channels with stronger LoS component.

V. Conclusion

We considered an UAV-enabled massive MIMO NOMA FD TWR system with multiple GU pairs, where the UAV employs low-precision ADCs/DACs antennas. Using MRC/MRT precoder and AQNM model, we derived the closed-form expressions of sum SE and total EE for imperfect CSI and imperfect SIC conditions. The impact of key system parameters on the SE performance was studied based on asymptotic analysis. The power scaling law was also characterized. We showed that the SE loss due to quantization noise can be effectively compensated by adjusting the UAV altitude and increasing the number of antennas. In addition, we confirmed that as the number of quantization bits increases, the sum SE increases until saturation is reached, while the EE initially increases and then deteriorates, and illustrate the optimal number of quantization bits and antennas needed to maximize EE. The SE/EE trade-off region grows with increasing Rician factor. As a result, UAV-enabled massive MIMO NOMA FD TWR systems can achieve considerable performance while saving energy by employing the low-resolution ADC/DAC architecture. Moreover, the utilization of low-precision ADCs/DACs is mainly used to reduce the energy consumption of multi-antenna UAV-assisted massive MIMO systems by changing the hardware configuration, and user scheduling and resource allocation as well as UAV flight trajectory optimization can also be considered to maximize the EE, which will be set aside in our future work.

Appendix A
Proof of Lemma 1

We here only provide the derivation of $\hat{\boldsymbol{H}}_{\rm SR}$ and $\boldsymbol{\Xi}_{\rm SR}$, since $\hat{\boldsymbol{H}}_{\rm RS}$ and $\boldsymbol{\Xi}_{\rm RS}$ can be deduced in the same fashion.

We first remove the known deterministic LoS components in (5), and obtain

$$\tilde{\boldsymbol{Y}}_{\rm rp} = \frac{\alpha_r \sqrt{P_\Phi}\tilde{\boldsymbol{H}}_{\rm SR}\sqrt{\boldsymbol{A}_\Phi}\boldsymbol{\Phi}}{\sqrt{(\boldsymbol{\Omega}_{\rm SR}+\boldsymbol{I}_{2M})}} + \alpha_r \boldsymbol{N}_{\rm rp} + \boldsymbol{N}_{\rm rq}, \tag{38}$$

where $\tilde{\boldsymbol{H}}_{\rm SR} = \left[\tilde{\boldsymbol{h}}_{{\rm SR},1}, \tilde{\boldsymbol{h}}_{{\rm SR},2}, ..., \tilde{\boldsymbol{h}}_{{\rm SR},2M}\right]$, $\tilde{\boldsymbol{h}}_{{\rm SR},i} = \beta_{{\rm SR},i}\tilde{\boldsymbol{g}}_{{\rm SR},i}$, $i \in [1, 2M]$, and $\boldsymbol{\Omega}_{\rm SR} = {\rm diag}\left(K_{{\rm SR},1}, K_{{\rm SR},2}, \ldots, K_{{\rm SR},2M}\right)$. Denote $\tilde{\boldsymbol{\Phi}}_{\rm rp} = \sqrt{(\boldsymbol{\Omega}_{\rm SR}+\boldsymbol{I}_{2M})^{-1}}\boldsymbol{\Phi}$, and from (38), we obtain

$$\tilde{\boldsymbol{Y}}_{\rm rp}^{\rm H} = \alpha_r \sqrt{P_\Phi}\tilde{\boldsymbol{\Phi}}_{\rm rp}^{\rm H}\sqrt{\boldsymbol{A}_\Phi^{\rm H}}\tilde{\boldsymbol{H}}_{\rm SR}^{\rm H} + \alpha_r \boldsymbol{N}_{\rm rp}^{\rm H} + \boldsymbol{N}_{\rm rq}^{\rm H}. \tag{39}$$

According to the standard MMSE estimation, the estimated $\tilde{\boldsymbol{H}}_{\rm SR}^{\rm H}$ can be expressed as [18]

$$\tilde{\boldsymbol{H}}_{\rm SR,est.}^{\rm H} = \mathbb{E}\left\{\tilde{\boldsymbol{H}}_{\rm SR}^{\rm H}\tilde{\boldsymbol{Y}}_{\rm rp}\right\}\left(\mathbb{E}\left\{\tilde{\boldsymbol{Y}}_{\rm rp}^{\rm H}\tilde{\boldsymbol{Y}}_{\rm rp}\right\}\right)^{-1}\tilde{\boldsymbol{Y}}_{\rm rp}^{\rm H}. \tag{40}$$

Recalling that $\boldsymbol{R}_{\boldsymbol{N}_{\rm rq}} = \alpha_r(1-\alpha_r) \times {\rm diag}\left(P_\Phi \boldsymbol{H}_{\rm SR}\boldsymbol{A}_\Phi \boldsymbol{H}_{\rm SR}^{\rm H} + \boldsymbol{I}_N\right)$, and defining $\tau = 2M$, $\boldsymbol{D}_{\rm SR} = {\rm diag}\left(\beta_{{\rm SR},1}, \beta_{{\rm SR},2}, \ldots, \beta_{{\rm SR},2M}\right)$, we have

$$\begin{aligned}\mathbb{E}\left\{\tilde{\boldsymbol{H}}_{\rm SR}^{\rm H}\tilde{\boldsymbol{Y}}_{\rm rp}\right\} = \mathbb{E}\Big\{\alpha_r\big(\sqrt{P_\Phi}\tilde{\boldsymbol{H}}_{\rm SR}^{\rm H}\tilde{\boldsymbol{H}}_{\rm SR}\sqrt{\boldsymbol{A}_\Phi}\tilde{\boldsymbol{\Phi}}_{\rm rp} + \tilde{\boldsymbol{H}}_{\rm SR}^{\rm H}\boldsymbol{N}_{\rm rp} \\ + \tilde{\boldsymbol{H}}_{\rm SR}^{\rm H}\boldsymbol{N}_{\rm rq}\big)\Big\} = N\alpha_r\sqrt{\boldsymbol{A}_\Phi P_\Phi}\boldsymbol{D}_{\rm SR}\tilde{\boldsymbol{\Phi}}_{\rm rp},\end{aligned} \tag{41}$$

$$\begin{aligned}\mathbb{E}\left\{\tilde{\boldsymbol{Y}}_{\rm rp}^{\rm H}\tilde{\boldsymbol{Y}}_{\rm rp}\right\} &= \mathbb{E}\Big\{\alpha_r^2 P_\Phi \tilde{\boldsymbol{\Phi}}_{\rm rp}^{\rm H}\sqrt{\boldsymbol{A}_\Phi^{\rm H}}\tilde{\boldsymbol{H}}_{\rm SR}^{\rm H}\tilde{\boldsymbol{H}}_{\rm SR}\sqrt{\boldsymbol{A}_\Phi}\tilde{\boldsymbol{\Phi}}_{\rm rp} \\ &\quad + \alpha_r^2\boldsymbol{N}_{\rm rp}^{\rm H}\boldsymbol{N}_{\rm rp} + \boldsymbol{N}_{\rm rq}^{\rm H}\boldsymbol{N}_{\rm rq}\Big\} \\ &= N\alpha_r\boldsymbol{A}_\Phi P_\Phi \boldsymbol{D}_{\rm SR} + N\alpha_r\boldsymbol{I}_{2M}.\end{aligned} \tag{42}$$

Then, substituting (39), (41) and (42) into (40), we have

$$\tilde{\boldsymbol{H}}_{\rm SR,est.}^{\rm H} = \tilde{\boldsymbol{H}}_{\rm SR}^{\rm H}\tilde{\boldsymbol{D}}_{\rm SR} + \frac{\tilde{\boldsymbol{D}}_{\rm SR}\tilde{\boldsymbol{\Phi}}_{\rm rp}\boldsymbol{N}_{\rm rp}^{\rm H}}{\sqrt{\boldsymbol{A}_\Phi P_\Phi}} + \frac{\tilde{\boldsymbol{D}}_{\rm SR}\tilde{\boldsymbol{\Phi}}_{\rm rp}\boldsymbol{N}_{\rm rq}^{\rm H}}{\alpha_r\sqrt{\boldsymbol{A}_\Phi P_\Phi}}, \tag{43}$$

where $\tilde{\boldsymbol{D}}_{\rm SR} = \alpha_r\left(\boldsymbol{I}_{2M} + \boldsymbol{A}_\Phi^{-1}P_\Phi^{-1}\tilde{\boldsymbol{D}}_{\rm SR}^{-1}\right)^{-1}$.

Based on (43), the estimated channel $\boldsymbol{H}_{\rm SR}$ can be given as

$$\hat{\boldsymbol{H}}_{\rm SR} = \bar{\boldsymbol{H}}_{\rm SR}\sqrt{\frac{\boldsymbol{\Omega}_{\rm SR}}{(\boldsymbol{\Omega}_{\rm SR}+\boldsymbol{I}_{2M})}} + \tilde{\boldsymbol{H}}_{\rm SR,est.}\sqrt{\frac{1}{(\boldsymbol{\Omega}_{\rm SR}+\boldsymbol{I}_{2M})}}, \tag{44}$$

where $\bar{\boldsymbol{H}}_{\rm SR} = \left[\bar{\boldsymbol{h}}_{{\rm SR},1}, \bar{\boldsymbol{h}}_{{\rm SR},2}, ..., \bar{\boldsymbol{h}}_{{\rm SR},2M}\right]$, $\bar{\boldsymbol{h}}_{{\rm SR},i} = \beta_{{\rm SR},i}\bar{\boldsymbol{g}}_{{\rm SR},i}$, $i \in [1, 2M]$.

Finally, the channel estimation error matrix is given by $\boldsymbol{\Xi}_{\rm SR} = \hat{\boldsymbol{H}}_{\rm SR} - \boldsymbol{H}_{\rm SR}$. Since $\hat{\boldsymbol{h}}_{{\rm SR},i}$, $\boldsymbol{e}_{{\rm SR},i}$ are the ith columns of $\hat{\boldsymbol{H}}_{\rm SR}$ and $\boldsymbol{\Xi}_{\rm SR}$, the variance of elements of $\hat{\boldsymbol{h}}_{{\rm SR},i}$, $\boldsymbol{e}_{{\rm SR},i}$ can be obtained by calculating $\mathbb{E}\left\{\left|\left[\hat{\boldsymbol{H}}_{\rm SR}\right]_{ni} - \mathbb{E}\left\{\left[\hat{\boldsymbol{H}}_{\rm SR}\right]_{ni}\right\}\right|^2\right\}$ and $\mathbb{E}\left\{\left|\left[\boldsymbol{\Xi}_{\rm SR}\right]_{ni} - \mathbb{E}\left\{\left[\boldsymbol{\Xi}_{\rm SR}\right]_{ni}\right\}\right|^2\right\}$, respectively. As a result, this completes the proof of Lemma 1.

$$\mathbb{E}\left\{\left\|\boldsymbol{W}\boldsymbol{H}_{\mathrm{SR}}\boldsymbol{\varrho}^{1/2}\right\|_{\mathrm{F}}^2\right\}=\mathbb{E}\left\{\mathrm{Tr}\left(\boldsymbol{W}\hat{\boldsymbol{H}}_{\mathrm{SR}}\boldsymbol{\varrho}\hat{\boldsymbol{H}}_{\mathrm{SR}}^{\mathrm{H}}\boldsymbol{W}^{\mathrm{H}}\right)\right\}+\mathbb{E}\left\{\mathrm{Tr}\left(\boldsymbol{W}\boldsymbol{\Xi}_{\mathrm{SR}}\boldsymbol{\varrho}\boldsymbol{\Xi}_{\mathrm{SR}}^{\mathrm{H}}\boldsymbol{W}^{\mathrm{H}}\right)\right\}$$
$$\xrightarrow[N\to\infty]{a.s.} N^3\sum\nolimits_{i=1}^{2M}\varrho_{\hat{i}}\delta_{\mathrm{RS},i}\delta_{\mathrm{SR},\hat{i}}^2+N^2\sum\nolimits_{j=1}^{2M}\delta_{\mathrm{RS},j}\delta_{\mathrm{SR},\hat{j}}\sum\nolimits_{i=1}^{2M}\varrho_i\varsigma_{\mathrm{SR},i}. \tag{45}$$

$$\mathbb{E}\left\{\left\|\boldsymbol{W}\boldsymbol{H}_{\mathrm{RR}}\right\|_{\mathrm{F}}^2\right\}=\mathbb{E}\left\{\mathrm{Tr}\left(\boldsymbol{W}\boldsymbol{H}_{\mathrm{RR}}\boldsymbol{H}_{\mathrm{RR}}^{\mathrm{H}}\boldsymbol{W}^{\mathrm{H}}\right)\right\}\xrightarrow[N\to\infty]{a.s.}N^3\sigma_{\mathrm{RR}}^2\sum\nolimits_{i=1}^{2M}\delta_{\mathrm{RS},i}\delta_{\mathrm{SR},\hat{i}}. \tag{46}$$

$$\mathbb{E}\left\{\left\|\boldsymbol{W}\right\|_{\mathrm{F}}^2\right\}=\mathbb{E}\left\{\mathrm{Tr}\left(\boldsymbol{W}\boldsymbol{W}^{\mathrm{H}}\right)\right\}\xrightarrow[N\to\infty]{a.s.}N^2\sum\nolimits_{i=1}^{2M}\delta_{\mathrm{RS},i}\delta_{\mathrm{SR},\hat{i}}. \tag{47}$$

$$\mathbb{E}\left\{\left\|\boldsymbol{W}\boldsymbol{R}_{\boldsymbol{n}_{\mathrm{rq}}}^{1/2}\right\|_{\mathrm{F}}^2\right\}\xrightarrow[N\to\infty]{a.s.}\alpha_r\left(1-\alpha_r\right)N^2\sum\nolimits_{i=1}^{2M}\delta_{\mathrm{RS},i}\delta_{\mathrm{SR},i}\left(\varrho_iP_{\mathrm{S}}\delta_{\mathrm{SR},i}+N^{-1}P_{\mathrm{R}}\sigma_{\mathrm{RR}}^2+\sigma_{\mathrm{R}}^2+\sum\nolimits_{j=1}^{2M}\varrho_jP_{\mathrm{S}}\beta_{\mathrm{SR},j}\right). \tag{48}$$

$$\varepsilon\xrightarrow[N\to\infty]{a.s.}\sqrt{\frac{P_{\mathrm{R}}}{\left\{\begin{array}{l}\alpha_r^2\left[N^3P_{\mathrm{S}}\sum\nolimits_{i=1}^{2M}\varrho_i\delta_{\mathrm{RS},i}\delta_{\mathrm{SR},\hat{i}}^2+N^2\sum\nolimits_{j=1}^{2M}\delta_{\mathrm{RS},j}\delta_{\mathrm{SR},\hat{j}}\left(P_{\mathrm{S}}\sum\nolimits_{i=1}^{2M}\varrho_i\varsigma_{\mathrm{SR},i}+P_{\mathrm{R}}\sigma_{\mathrm{RR}}^2+\sigma_{\mathrm{R}}^2\right)\right]\\+\alpha_r\left(1-\alpha_r\right)N^2\sum\nolimits_{i=1}^{2M}\delta_{\mathrm{RS},i}\delta_{\mathrm{SR},i}\left(\varrho_iP_{\mathrm{S}}\delta_{\mathrm{SR},i}+P_{\mathrm{S}}\sum\nolimits_{j=1}^{2M}\varrho_j\beta_{\mathrm{SR},j}+N^{-1}P_{\mathrm{R}}\sigma_{\mathrm{RR}}^2+\sigma_{\mathrm{R}}^2\right)\end{array}\right\}}}. \tag{49}$$

Appendix B
Proof of Theorem 1

A. Derivation of ε

We calculate the terms $\mathbb{E}\left\{\left\|\boldsymbol{W}\boldsymbol{H}_{\mathrm{SR}}\boldsymbol{\varrho}^{1/2}\right\|_{\mathrm{F}}^2\right\}$, $\mathbb{E}\left\{\left\|\boldsymbol{W}\boldsymbol{H}_{\mathrm{RR}}\right\|_{\mathrm{F}}^2\right\}$, $\mathbb{E}\left\{\left\|\boldsymbol{W}\right\|_{\mathrm{F}}^2\right\}$ and $\mathbb{E}\left\{\left\|\boldsymbol{W}\boldsymbol{R}_{\boldsymbol{n}_{\mathrm{rq}}}^{1/2}\right\|_{\mathrm{F}}^2\right\}$. The expressions are given at the top of this page, and taking the derived results into (15), we obtain ε, as shown in (49).

B. Derivation of $\gamma_{m,\hat{m}}$

To obtain Theorem 1, we need to calculate (17). Firstly, there is

$$\mathbb{E}\left\{\boldsymbol{h}_{\mathrm{RS},m}^{\mathrm{T}}\boldsymbol{F}\boldsymbol{h}_{\mathrm{SR},\hat{m}}\right\}=\mathbb{E}\left\{\hat{\boldsymbol{h}}_{\mathrm{RS},m}^{\mathrm{T}}\boldsymbol{F}\hat{\boldsymbol{h}}_{\mathrm{SR},\hat{m}}\right\}+\mathbb{E}\left\{\boldsymbol{e}_{\mathrm{RS},m}^{\mathrm{T}}\boldsymbol{F}\boldsymbol{e}_{\mathrm{SR},\hat{m}}\right\}$$
$$=N^2\varepsilon^2\delta_{\mathrm{RS},m}\delta_{\mathrm{SR},\hat{m}}. \tag{50}$$

Next, for any i, we have

$$\mathbb{E}\left\{\left|\boldsymbol{h}_{\mathrm{RS},m}^{\mathrm{T}}\boldsymbol{F}\boldsymbol{h}_{\mathrm{SR},i}\right|^2\right\}$$
$$=\mathbb{E}\left\{\left|\hat{\boldsymbol{h}}_{\mathrm{RS},m}^{\mathrm{T}}\boldsymbol{F}\hat{\boldsymbol{h}}_{\mathrm{SR},i}\right|^2\right\}+\varsigma_{\mathrm{SR},i}\mathbb{E}\left\{\left\|\hat{\boldsymbol{h}}_{\mathrm{RS},m}^{\mathrm{T}}\boldsymbol{F}\right\|^2\right\} \tag{51}$$
$$+\varsigma_{\mathrm{RS},m}\mathbb{E}\left\{\left\|\boldsymbol{F}\hat{\boldsymbol{h}}_{\mathrm{SR},i}\right\|^2\right\}+\varsigma_{\mathrm{RS},m}\varsigma_{\mathrm{SR},i}\mathbb{E}\left\{\left\|\boldsymbol{F}\right\|^2\right\}.$$

where

$$\mathbb{E}\left\{\left|\hat{\boldsymbol{h}}_{\mathrm{RS},m}^{\mathrm{T}}\boldsymbol{F}\hat{\boldsymbol{h}}_{\mathrm{SR},i}\right|^2\right\}=\varepsilon^2\mathbb{E}\left\{\left|\hat{\boldsymbol{h}}_{\mathrm{RS},m}^{\mathrm{T}}\boldsymbol{W}\hat{\boldsymbol{h}}_{\mathrm{SR},i}\right|^2\right\}$$
$$=\varepsilon^2\sum\nolimits_{j=1}^{2M}\psi_{\mathrm{RS},mj}\psi_{\mathrm{SR},\hat{j}i}, \tag{52}$$

$$\mathbb{E}\left\{\left\|\hat{\boldsymbol{h}}_{\mathrm{RS},m}^{\mathrm{T}}\boldsymbol{F}\right\|^2\right\}=\varepsilon^2\mathbb{E}\left\{\mathrm{Tr}\left(\hat{\boldsymbol{h}}_{\mathrm{RS},m}^{\mathrm{T}}\boldsymbol{W}\boldsymbol{W}^{\mathrm{H}}\hat{\boldsymbol{h}}_{\mathrm{RS},m}^{*}\right)\right\}$$
$$=N\varepsilon^2(\delta_{\mathrm{SR},\hat{m}}\psi_{\mathrm{RS},mm}+\delta_{\mathrm{SR},m}\psi_{\mathrm{RS},m\hat{m}}), \tag{53}$$

$$\mathbb{E}\left\{\left\|\boldsymbol{F}\hat{\boldsymbol{h}}_{\mathrm{SR},i}\right\|^2\right\}=\varepsilon^2\mathbb{E}\left\{\mathrm{Tr}\left(\boldsymbol{W}\hat{\boldsymbol{h}}_{\mathrm{SR},i}\hat{\boldsymbol{h}}_{\mathrm{SR},i}^{\mathrm{H}}\boldsymbol{W}^{\mathrm{H}}\right)\right\}$$
$$=N\varepsilon^2(\delta_{\mathrm{RS},\hat{i}}\psi_{\mathrm{SR},ii}+\delta_{\mathrm{RS},i}\psi_{\mathrm{SR},\hat{i}i}), \tag{54}$$

$$\mathbb{E}\left\{\left\|\boldsymbol{F}\right\|^2\right\}=\varepsilon^2\mathbb{E}\left\{\mathrm{Tr}\left(\boldsymbol{W}\boldsymbol{W}^{\mathrm{H}}\right)\right\}=N^2\varepsilon^2\sum\nolimits_{j=1}^{2M}\delta_{\mathrm{RS},j}\delta_{\mathrm{SR},\hat{j}}. \tag{55}$$

Since $\mathbb{V}\mathrm{ar}\left(\boldsymbol{h}_{\mathrm{RS},m}^{\mathrm{T}}\boldsymbol{F}\boldsymbol{h}_{\mathrm{SR},\hat{m}}\right)=\mathbb{E}\left\{\left|\boldsymbol{h}_{\mathrm{RS},m}^{\mathrm{T}}\boldsymbol{F}\boldsymbol{h}_{\mathrm{SR},\hat{m}}\right|^2\right\}-\left|\mathbb{E}\left\{\boldsymbol{h}_{\mathrm{RS},m}^{\mathrm{T}}\boldsymbol{F}\boldsymbol{h}_{\mathrm{SR},\hat{m}}\right\}\right|^2$, combining (50) and (51), we can calculate $L_{1_{m,\hat{m}}}$. According to (51), we can get $L_{2_{m,\hat{m}}}$.

Furthermore, $\mathbb{E}\left\{\left|\boldsymbol{h}_{\mathrm{RS},m}^{\mathrm{T}}\boldsymbol{F}\boldsymbol{h}_{\mathrm{SR},m}-\hat{\boldsymbol{h}}_{\mathrm{RS},m}^{\mathrm{T}}\boldsymbol{F}\hat{\boldsymbol{h}}_{\mathrm{SR},m}\right|^2\right\}=\varsigma_{\mathrm{SR},m}\mathbb{E}\left\{\left\|\hat{\boldsymbol{h}}_{\mathrm{RS},m}^{\mathrm{T}}\boldsymbol{F}\right\|^2\right\}+\varsigma_{\mathrm{RS},m}\mathbb{E}\left\{\left\|\boldsymbol{F}\hat{\boldsymbol{h}}_{\mathrm{SR},m}\right\|^2\right\}+\varsigma_{\mathrm{SR},m}\varsigma_{\mathrm{RS},m}\times\mathbb{E}\left\{\left\|\boldsymbol{F}\right\|^2\right\}$, substituting (53), (54) and (55), we obtain $L_{3_{m,\hat{m}}}$.

Moreover, $\mathbb{E}\left\{\left\|\boldsymbol{h}_{\mathrm{RS},m}^{\mathrm{T}}\boldsymbol{F}\boldsymbol{H}_{\mathrm{RR}}\right\|^2\right\}=\sigma_{\mathrm{RR}}^2\mathbb{E}\left\{\left\|\boldsymbol{h}_{\mathrm{RS},m}^{\mathrm{T}}\boldsymbol{F}\right\|^2\right\}$, $\mathbb{E}\left\{\left\|\boldsymbol{h}_{\mathrm{RS},m}^{\mathrm{T}}\boldsymbol{F}\right\|^2\right\}=\mathbb{E}\left\{\left\|\hat{\boldsymbol{h}}_{\mathrm{RS},m}^{\mathrm{T}}\boldsymbol{F}\right\|^2\right\}+\mathbb{E}\left\{\left\|\boldsymbol{F}\boldsymbol{e}_{\mathrm{SR},i}\right\|^2\right\}$, substituting (53) and (55), we obtain $L_{4_{m,\hat{m}}}$ and $L_{6_{m,\hat{m}}}$.

Finally, we derive $L_{5_{m,\hat{m}}}$, i.e., $\mathbb{E}\left\{\left\|\boldsymbol{h}_{\mathrm{RS},m}^{\mathrm{T}}\boldsymbol{F}\boldsymbol{n}_{\mathrm{rq}}\right\|^2\right\}$ and $\mathbb{E}\left\{\left\|\boldsymbol{h}_{\mathrm{RS},m}^{\mathrm{T}}\boldsymbol{n}_{\mathrm{tq}}\right\|^2\right\}$, which are given by

$$\mathbb{E}\left\{\left\|\boldsymbol{h}_{\mathrm{RS},m}^{\mathrm{T}}\boldsymbol{F}\boldsymbol{n}_{\mathrm{rq}}\right\|^2\right\}=\varepsilon^2\mathbb{E}\left\{\left\|\hat{\boldsymbol{h}}_{\mathrm{RS},m}^{\mathrm{T}}\boldsymbol{W}\boldsymbol{n}_{\mathrm{rq}}\right\|^2\right\}$$
$$+\varepsilon^2\varsigma_{\mathrm{RS},m}\mathbb{E}\left\{\left\|\boldsymbol{W}\boldsymbol{n}_{\mathrm{rq}}\right\|^2\right\}, \tag{56}$$

where $\mathbb{E}\left\{\left\|\hat{\boldsymbol{h}}_{\mathrm{RS},m}^{\mathrm{T}}\boldsymbol{W}\boldsymbol{n}_{\mathrm{rq}}\right\|^2\right\}$ is given by (57) at the top of next

$$\begin{aligned}\mathbb{E}\left\{\left\|\hat{\boldsymbol{h}}_{\mathrm{RS},m}^{\mathrm{T}}\boldsymbol{W}\boldsymbol{n}_{\mathrm{rq}}\right\|^2\right\} &= \sum\nolimits_{i=1}^{2M}\mathbb{E}\left\{\mathrm{Tr}\left(\hat{\boldsymbol{h}}_{\mathrm{RS},m}^{\mathrm{T}}\hat{\boldsymbol{h}}_{\mathrm{RS},i}^{*}\hat{\boldsymbol{h}}_{\mathrm{SR},\hat{\imath}}^{\mathrm{H}}\boldsymbol{n}_{\mathrm{rq}}\boldsymbol{n}_{\mathrm{rq}}^{\mathrm{H}}\hat{\boldsymbol{h}}_{\mathrm{SR},\hat{\imath}}\hat{\boldsymbol{h}}_{\mathrm{RS},i}^{\mathrm{T}}\hat{\boldsymbol{h}}_{\mathrm{RS},m}^{*}\right)\right\}\\ &= \mathbb{E}\left\{\mathrm{Tr}\left(\hat{\boldsymbol{h}}_{\mathrm{RS},m}^{\mathrm{T}}\hat{\boldsymbol{h}}_{\mathrm{RS},m}^{*}\hat{\boldsymbol{h}}_{\mathrm{SR},\hat{m}}^{\mathrm{H}}\boldsymbol{n}_{\mathrm{rq}}\boldsymbol{n}_{\mathrm{rq}}^{\mathrm{H}}\hat{\boldsymbol{h}}_{\mathrm{SR},\hat{m}}\hat{\boldsymbol{h}}_{\mathrm{RS},m}^{\mathrm{T}}\hat{\boldsymbol{h}}_{\mathrm{RS},m}^{*}\right)\right\}\\ &+ \sum\nolimits_{i=1,i\neq m}^{2M}\mathbb{E}\left\{\mathrm{Tr}\left(\hat{\boldsymbol{h}}_{\mathrm{RS},m}^{\mathrm{T}}\hat{\boldsymbol{h}}_{\mathrm{RS},i}^{*}\hat{\boldsymbol{h}}_{\mathrm{SR},\hat{\imath}}^{\mathrm{H}}\boldsymbol{n}_{\mathrm{rq}}\boldsymbol{n}_{\mathrm{rq}}^{\mathrm{H}}\hat{\boldsymbol{h}}_{\mathrm{SR},\hat{\imath}}\hat{\boldsymbol{h}}_{\mathrm{RS},i}^{\mathrm{T}}\hat{\boldsymbol{h}}_{\mathrm{RS},m}^{*}\right)\right\}\\ &= \alpha_r\left(1-\alpha_r\right)N\sum\nolimits_{i=1}^{2M}\psi_{\mathrm{RS},im}\delta_{\mathrm{SR},\hat{\imath}}\left(N^{-1}P_{\mathrm{R}}\sigma_{\mathrm{RR}}^2+\sigma_{\mathrm{R}}^2+P_{\mathrm{S}}\sum\nolimits_{j=1}^{2M}\varrho_j\beta_{\mathrm{SR},j}+\varrho_{\hat{\imath}}P_{\mathrm{S}}\delta_{\mathrm{SR},\hat{\imath}}\right).\end{aligned} \tag{57}$$

page. $\mathbb{E}\left\{\|\boldsymbol{W}\boldsymbol{n}_{\mathrm{rq}}\|^2\right\}$ can be obtained in the same way.

$$\begin{aligned}\mathbb{E}\left\{\left\|\boldsymbol{h}_{\mathrm{RS},m}^{\mathrm{T}}\boldsymbol{n}_{\mathrm{tq}}\right\|^2\right\} &= \mathbb{E}\left\{\left\|\hat{\boldsymbol{h}}_{\mathrm{RS},m}^{\mathrm{T}}\boldsymbol{n}_{\mathrm{tq}}\right\|^2\right\}+\mathbb{E}\left\{\left\|\boldsymbol{e}_{\mathrm{RS},m}^{\mathrm{T}}\boldsymbol{n}_{\mathrm{tq}}\right\|^2\right\}\\ &= \alpha_t\left(1-\alpha_t\right)P_{\mathrm{R}}\left(\delta_{\mathrm{RS},m}+N^{-1}\varsigma_{\mathrm{RS},m}\right).\end{aligned} \tag{58}$$

As a result, Theorem 1 is concluded with the derived results.

REFERENCES

[1] N. Zhao, W. Lu, M. Sheng, Y. Chen, J. Tang, F. R. Yu, and K.-K. Wong, "UAV-Assisted Emergency Networks in Disasters," *IEEE Wireless Commun.*, vol. 26, no. 1, pp. 45–51, Feb. 2019.

[2] J. Wang, Z. Na, and X. Liu, "Collaborative Design of Multi-UAV Trajectory and Resource Scheduling for 6G-Enabled Internet of Things," *IEEE Internet of Things J.*, vol. 8, no. 20, pp. 15 096–15 106, Oct. 2021.

[3] J. Li, Y. Liu, X. Li, C. Shen, and Y. Chen, "Non-Orthogonal Multiple Access in Cooperative UAV Networks: A Stochastic Geometry Model," in *2019 IEEE 90th Vehicular Technology Conference (VTC2019-Fall)*, Honolulu, HI, USA, Sep. 2019, pp. 1–6.

[4] Q. Wang, X. Li, S. Bhatia, Y. Liu, L. T. Alex, S. A. Khowaja, and V. G. Menon, "UAV-Enabled Non-Orthogonal Multiple Access Networks for Ground-Air-Ground Communications," *IEEE Trans. Green Commun. Netw.*, vol. 6, no. 3, pp. 1340–1354, Sep. 2022.

[5] D. W. Matolak and R. Sun, "Air-Ground Channel Characterization for Unmanned Aircraft Systems-Part III: The Suburban and Near-Urban Environments," *IEEE Trans. Veh. Technol.*, vol. 66, no. 8, pp. 6607–6618, Aug. 2017.

[6] H. Q. Ngo, E. G. Larsson, and T. L. Marzetta, "Energy and Spectral Efficiency of Very Large Multiuser MIMO Systems," *IEEE Trans. Commun.*, vol. 61, no. 4, pp. 1436–1449, Apr. 2013.

[7] J. Zhang, Y. Zhang, Y. Yu, R. Xu, Q. Zheng, and P. Zhang, "3-D MIMO: How Much Does It Meet Our Expectations Observed From Channel Measurements?" *IEEE J. Sel. Areas Commun.*, vol. 35, no. 8, pp. 1887–1903, Aug. 2017.

[8] X. Li, J. Li, Y. Liu, Z. Ding, and A. Nallanathan, "Residual Transceiver Hardware Impairments on Cooperative NOMA Networks," *IEEE Trans. Wireless Commun.*, vol. 19, no. 1, pp. 680–695, Jan. 2020.

[9] X. Li, Q. Wang, M. Zeng, Y. Liu, S. Dang, T. A. Tsiftsis, and O. A. Dobre, "Physical-layer authentication for ambient backscatter-aided noma symbiotic systems," *IEEE Trans. Commun.*, pp. 1–1, 2023.

[10] X. Wang, D. Zhang, K. Xu, and C. Yuan, "On the sum rate of multi-user full-duplex massive MIMO systems," in *2016 IEEE International Conference on Communication Systems (ICCS)*, Shenzhen, China, Dec. 2016, pp. 1–7.

[11] Y. Liang, L. Xiao, D. Yang, Y. Liu, and T. Zhang, "Joint Trajectory and Resource Optimization for UAV-Aided Two-Way Relay Networks," *IEEE Trans. Veh. Technol.*, vol. 71, no. 1, pp. 639–652, Jan. 2022.

[12] G. Geraci, A. Garcia-Rodriguez, L. G. Giordano, D. Lopez-Perez, and E. Bjoernson, "Supporting UAV Cellular Communications through Massive MIMO," in *2018 IEEE International Conference on Communications Workshops (ICC Workshops)*, Kansas City, MO, USA, May 2018, pp. 1–6.

[13] J. Du, W. Xu, Y. Deng, A. Nallanathan, and L. Vandendorpe, "Energy-Saving UAV-Assisted Multiuser Communications With Massive MIMO Hybrid Beamforming," *IEEE Commun. Lett.*, vol. 24, no. 5, pp. 1100–1104, May 2020.

[14] F. Zhu, Z. Wang, W. Feng, J. Tang, Y. Liu, and X. Zhang, "Joint 3D Placement and Power Allocation for UAV-aided MIMO-NOMA Networks," in *2020 IEEE/CIC International Conference on Communications in China (ICCC)*, Chongqing, China, Aug. 2020, pp. 663–668.

[15] J. Singh, O. Dabeer, and U. Madhow, "On the limits of communication with low-precision analog-to-digital conversion at the receiver," *IEEE Trans. Commun.*, vol. 57, no. 12, pp. 3629–3639, Dec. 2009.

[16] A. Mezghani, R. Ghiat, and J. A. Nossek, "Transmit processing with low resolution D/A-converters," in *2009 16th IEEE International Conference on Electronics, Circuits and Systems - (ICECS 2009)*, Yasmine Hammamet, Tunisia, Dec. 2009, pp. 683–686.

[17] X. Jia, M. Zhou, M. Xie, L. Yang, and H. Zhu, "Effect of Low-Resolution ADCs and Loop Interference on Multi-User Full-Duplex Massive MIMO Amplify-and-Forward Relaying Systems," *IET Commun.*, vol. 11, no. 5, pp. 687–695, Mar. 2017.

[18] C. Kong, C. Zhong, S. Jin, S. Yang, H. Lin, and Z. Zhang, "Full-Duplex Massive MIMO Relaying Systems With Low-Resolution ADCs," *IEEE Trans. Wireless Commun.*, vol. 16, no. 8, pp. 5033–5047, Aug. 2017.

[19] X. Yu, J. Dai, X. Yin, and Z. Jiang, "Full-Duplex Massive MIMO Relaying Systems with Low-Resolution ADCs over Rician Fading Channels," *IET Commun.*, vol. 13, no. 18, pp. 3088–3096, Nov. 2019.

[20] P. Anokye, R. K. Ahiadormey, H.-S. Jo, C. Song, and K.-J. Lee, "Low-Resolution ADC Quantized Full-Duplex Massive MIMO-Enabled Wireless Backhaul in Heterogeneous Networks Over Rician Channels," *IEEE Trans. Wireless Commun.*, vol. 19, no. 8, pp. 5503–5517, Aug. 2020.

[21] J. Dai, J. Liu, J. Wang, R. Song, and C. Cheng, "Asymptotic Analysis of Full-Duplex Large-Scale MIMO Systems With Low-Resolution ADCs/DACs Over Rician Fading Channels," *IEEE Syst. J.*, vol. 14, no. 4, pp. 4832–4841, Dec. 2020.

[22] Q. Ding, Y. Lian, and Y. Jing, "Performance Analysis of Full-Duplex Massive MIMO Systems With Low-Resolution ADCs/DACs Over Rician Fading Channels," *IEEE Trans. Veh. Technol.*, vol. 69, no. 7, pp. 7389–7403, Jul. 2020.

[23] A. Al-Hourani, S. Kandeepan, and S. Lardner, "Optimal LAP Altitude for Maximum Coverage," *IEEE Wireless Commun. Lett.*, vol. 3, no. 6, pp. 569–572, Dec. 2014.

[24] E. Everett, A. Sahai, and A. Sabharwal, "Passive Self-Interference Suppression for Full-Duplex Infrastructure Nodes," *IEEE Trans. Wireless Commun.*, vol. 13, no. 2, pp. 680–694, Feb. 2014.

[25] M. A. Ahmed, C. C. Tsimenidis, and A. F. Al Rawi, "Performance Analysis of Full-Duplex-MRC-MIMO With Self-Interference Cancellation Using Null-Space-Projection," *IEEE Trans. Signal Process.*, vol. 64, no. 12, pp. 3093–3105, Jun. 2016.

[26] J. Zhang, L. Dai, Z. He, S. Jin, and X. Li, "Performance Analysis of Mixed-ADC Massive MIMO Systems Over Rician Fading Channels," *IEEE J. Sel. Areas Commun.*, vol. 35, no. 6, pp. 1327–1338, Jun. 2017.

[27] Z. Wang, Y. Wu, Y. Cai, J. Wang, and G. Yue, "Robust MMSE-Based Beamforming for Massive MIMO Multi-Pair Two-Way Relay Systems with Low-Resolution ADCs/DACs," in *2021 13th International Conference on Wireless Communications and Signal Processing (WCSP)*, Changsha, China, Oct. 2021, pp. 1–6.

[28] M. Ji, J. Chen, L. Lv, and H. Tang, "Nonorthogonal Multiple Access Enabled Two-Way Relay System Using Signal Alignment," *IEEE Syst. J.*, vol. 16, no. 4, pp. 5765–5776, Dec. 2022.

[29] J. Zhang, L. Dai, Z. He, B. Ai, and O. A. Dobre, "Mixed-ADC/DAC Multipair Massive MIMO Relaying Systems: Performance Analysis and Power Optimization," *IEEE Trans. Commun.*, vol. 67, no. 1, pp. 140–153, Jan. 2019.

[30] C. He, B. Sheng, P. Zhu, D. Wang, and X. You, "Energy efficiency comparison between distributed and co-located MIMO systems," *Int.J. Commun. Syst.*, vol. 27, no. 1, pp. 81–94, Mar. 2014.

[31] S. Cui, A. Goldsmith, and A. Bahai, "Energy-constrained modulation optimization," *IEEE Trans. Wireless Commun.*, vol. 4, no. 5, pp. 2349–2360, Sep. 2005.